JOURNAL OF GEOPHYSICAL RESEARCH, VOL. 105, NO. D12, PAGES 15,627–15,652, JUNE 27, 2000

Comparisons of aircraft, ship, and buoy radiation and SST measurements from TOGA COARE

Sean P. Burns,[1,2] Djamal Khelif,[1] Carl A. Friehe,[1] Phil Hignett,[3]
Alastair G. Williams,[4] Alan L. M. Grant,[4] Jörg M. Hacker,[5]
Denise E. Hagan,[6] Yolande L. Serra,[7] David P. Rogers,[8] E. Frank Bradley,[9]
Robert A. Weller,[10] Chris W. Fairall,[11] Steven P. Anderson,[10]
Clayton A. Paulson,[12] and Peter A. Coppin[9]

Abstract. Mean radiative fluxes and sea surface temperature measured by the five Tropical Ocean-Global Atmosphere Coupled Ocean-Atmosphere Response Experiment (TOGA COARE) boundary layer research aircraft were compared with each other and with surface measurements from moored buoys and ships. The basic data-processing techniques for radiative flux and sea surface temperature (SST) measurements from an aircraft were reviewed, and an empirical optimization method to calibrate an Eppley pyrgeometer was introduced. On the basis of aircraft wingtip-to-wingtip comparison periods, the processed aircraft downwelling shortwave and longwave irradiance and SST measurements were found to agree to 28±18 W m^{-2}, 9±4 W m^{-2}, and 0.7±0.4°C, respectively. By using the same comparison periods, empirical corrections that removed systematic errors in the aircraft data were determined. Application of these corrections improved the wingtip comparison accuracy to 3±16 W m^{-2}, 1±4 W m^{-2}, and 0.1±0.3°C, respectively. Comparisons between the (fully corrected) aircraft and the surface platform measurements revealed the aircraft data to be slightly greater for all three parameters. The agreement was around 3±37 W m^{-2}, 3±6 W m^{-2}, and 0.3±0.5°C for shortwave irradiance, longwave irradiance, and SST, respectively. (Detailed comparison results were provided for each individual ship and buoy.) After applying the aircraft empirical corrections the level of accuracy was near the COARE objectives.

[1]Department of Mechanical and Aerospace Engineering, University of California, Irvine.

[2]Now at Mesoscale and Microscale Meteorology Division, National Center for Atmospheric Research, Boulder, Colorado.

[3]Meteorological Support Group/DG(R&T), Ministry of Defence, London, England.

[4]Hadley Centre for Climate Prediction and Research, Berkshire, England.

[5]Flinders Institute for Atmospheric and Marine Sciences, Adelaide, Australia.

[6]Jet Propulsion Laboratory, Pasadena, California.

[7]Department of Atmospheric Science, University of Washington, Seattle.

[8]Scripps Institution of Oceanography, La Jolla, California.

[9]Commonwealth Scientific and Industrial Research Organization Land and Water, Canberra, Australia.

[10]Woods Hole Oceanographic Institution, Woods Hole, Massachusetts.

[11]Environmental Technology Laboratory, Boulder, Colorado.

[12]College of Oceanic and Atmospheric Sciences, Oregon State University, Corvallis.

Copyright 2000 by the American Geophysical Union.

Paper number 2000JD900090.
0148-0227/00/2000JD900090$09.00

1. Introduction

A component of the Tropical Ocean-Global Atmosphere Coupled Ocean-Atmosphere Response Experiment (TOGA COARE) was the measurement of radiative fluxes and sea surface temperature (SST) [*Webster and Lukas*, 1992]. Five research aircraft were used in COARE during the intensive observing period (IOP) between November 1, 1992 and February 28, 1993, to measure upward and downward shortwave (Q_{SW}) and longwave (Q_{LW}) irradiance (i.e., radiative flux through the horizontal plane) and infer SST from narrowband infrared radiometers. A goal of COARE was to determine the net surface shortwave and longwave radiative fluxes to within ±6-7 W m^{-2} [*Fairall et al.*, 1998] and measure SST to an accuracy of ±0.2°C [*Fairall et al.*, 1996b]. The objectives of this paper are (1) to determine empirical corrections for the aircraft data on the basis of aircraft wingtip-to-wingtip comparisons and consideration of the ship and buoy data and (2) to assess the in situ accuracies of the aircraft, ship, and buoy data.

The five boundary layer aircraft deployed in COARE were the two National Oceanic and Atmospheric Administration (NOAA) WP-3D Orions (N42RF and N43RF), the National Center for Atmospheric Research

(NCAR) Electra N308D, the Meteorological Research Flight (MRF) C130, and the Flinders Institute for Atmospheric and Marine Sciences (FIAMS) Cessna 340A. Detailed information on the surface platforms used for the comparisons can be found in the work of *Burns et al.* [1999], and a summary of the aircraft and surface platform instrumentation relative to the present study is given in Table 1.

Table 1. Radiation-Measuring Instrumentation on Aircraft and Surface Platforms Used in TOGA COARE Data Comparisons.

Platform	Sea Surface Temperature[a]	Shortwave Irradiance[b]	Longwave Irradiance[c]	SI[d]
		Research Aircraft		
NOAA WP-3D N42RF (N42RF)	Barnes PRT-5, 9.5-11 μm ($\pm$ 0.5°C)	Eppley PSP ($\pm$ 1%)	Eppley PIR ($\pm$ 2%)	1 s
NOAA WP-3D N43RF (N43RF)	Barnes PRT-5, 9.5-11 μm ($\pm$ 0.5°C)	Eppley PSP ($\pm$ 1%)	Eppley PIR ($\pm$ 2%)	1 s
NCAR Electra N308D (N308D)	Barnes PRT-5, 8-14 μm & JPL[e] 10-12 μm ($\pm$ 1.0°C, $\pm$ 0.3°C)	Eppley PSP, (RAF-modified) ($\pm$ 1%)	Eppley PIR, (RAF-modified) ($\pm$ 1%)	1 s
MRF UK C130 (C130)	Barnes PRT-4 (MRF-modified), 8-14 μm ($\pm$ 0.6°C)	Eppley PSP, 0.3-3 μm ($\pm$ 3%)	MRF Design, 4-50 μm ($\pm$ 10 W m^{-2})	1 s
FIAMS Cessna 340A (340A)	Heimann KT-15, 8-14 μm ($\pm$ 0.5°C)	Eppley PSP ($\pm$ 1%)	Eppley PIR ($\pm$ 2%)	1 s[f]
		Research Vessels (R/V)		
USN/UH *Moana Wave* (WAVE)	YSI Thermistor (46040), floating, at 0.05 m depth ($\pm$ 0.2°C)	Eppley PSP, at 15 m ($\pm$ 4 W m^{-2})	Eppley PIR, at 15 m ($\pm$ 2.5 W m^{-2})	$\sim$ 10 min
NSF/OSU *Wecoma*[g] (WECM)	"bucket" thermometer, at 0.2 m depth ($\pm$ 0.2°C)	Eppley PSP, port side, at 8 m ($\pm$ 4 W m^{-2})	Eppley PIR, port side, at 8 m ($\pm$ 5 W m^{-2})	30 min
CSIRO *Franklin*[h] (FRNK)	Thermosalinograph (Ocean Data TSG 103), at 1 m depth[i] ($\pm$ 0.1°C)	Eppley PSP, at 20 m ($\pm$ 3 W m^{-2})	Eppley PIR, at 20 m ($\pm$ 5 W m^{-2})	15 min
		Research Moorings		
NOAA/PMEL ATLAS (ATLS)	YSI Thermistor (46006), at 1 m depth ($\pm$ 0.03°C)	NA	NA	60 min[j]
WHOI Mooring (IMET)	YSI Thermistor (46033) Brancker Model XX-105, at 0.45 m depth ($\pm$ 0.1°C)	Eppley PSP, at 3.54 m ($\pm$ 3 W m^{-2})	Eppley PIR, at 3.54 m ($\pm$ 10 W m^{-2})	7.5 min

Abbreviations for each platform and estimated accuracies are in parentheses; NA, data not available. Acronyms used for the surface platforms: USN/UH (U.S. Navy, University of Hawaii), NSF/OSU (National Science Foundation, Oregon State University), CSIRO (Commonwealth Scientific and Industrial Research Organisation), PMEL (Pacific Marine Environmental Laboratory), and WHOI (Woods Hole Oceanographic Institution).

[a]PRT, precision radiation thermometer.

[b]PSP, precision spectral pyranometer (model PSP), passband = 0.285-2.8 μm.

[c]PIR, precision infrared radiometer, or pyrgeometer (model PIR), passband = 3.5-50 μm.

[d]SI, time interval between samples.

[e]A radiometer built at the Jet Propulsion Laboratory (JPL).

[f]A 1-s boxcar average from 20-Hz data.

[g]Other SST sensor: SeaBird at the bow, at 2-m depth.

[h]Other SST sensors: CSIRO/Rutherford-Appleton infrared radiometer, SEASOAR.

[i]Thermosalinograph intake was at 2.4 m, but the water being measured originated from a depth of about 1 m.

[j]A 60-min boxcar average of data sampled every 10 min.

A previous comparison of COARE aircraft, buoy, and ship meteorological measurements by *Burns et al.* [1999] describes the comparison techniques and how to obtain data used in the present study. The WP-3D data used were processed at the University of California, Irvine (UCI). A good preliminary overview of COARE scientific findings is given by *Godfrey et al.* [1998], although it should be noted that they list differences between aircraft and surface platform measurements which are different from the present findings. Empirical corrections to the COARE aircraft SST data, which are similar to the present findings, have been used by other investigators [*LeMone et al.*, 1998; *Vickers and Esbensen*, 1998; *Walsh et al.*, 1998]. An examination of the surface energy budget using C130 data has been performed by *Grant and Hignett* [1998]. Other studies of the tropical boundary layer and sea surface temperature using COARE aircraft (*Williams et al.* [1996, 1997] (340A), *Serra et al.* [1997] (N308D), and *Hagan et al.* [1997] (N308D)) provide more information about the aircraft instrumentation, data collected, and meteorological conditions during the flights. The current study consolidates aircraft data from these previous studies and summarizes how data from each aircraft compare with one another.

Radiative flux data measured by three aircraft at high altitude (~6 km) have been compared during a single clear-sky flight by *Saunders et al.* [1992], who found agreement of within 2% for the upwelling and downwelling shortwave fluxes and a maximum difference of 7% for the upwelling Q_{LW} measurements. A two-aircraft comparison at 3.7 km by *Valero et al.* [1997], shows agreement over four level legs in downwelling shortwave flux to be better than 0.1% (~2.4 W m^{-2}) on average. Previous high-altitude comparisons of multiple pyranometers and pyrgeometers, mounted on the C130, resulted in 0.6% (6 W m^{-2}) agreement in downwelling Q_{SW} and 11% (10 W m^{-2}) and 4% (12 W m^{-2}) agreement for downwelling and upwelling Q_{LW}, respectively [*Saunders and Barnes*, 1990]. In contrast to these high-altitude studies based on only a few flights, the present study includes comparisons from many flight missions and conditions spread over 4 months and emphasizes low-level (< 100 m) measurements during daylight hours in generally fair weather conditions.

Since the term "SST" is rather general, the following specific descriptions are used in this study: the raw measurement made by any infrared radiometer is designated T_{ir}, all subsurface temperature measurements T_m, and the actual air-sea interface (or "skin") temperature T_s. The skin temperature is usually a calculated quantity, based on other measurements. For example, to calculate T_s from T_{ir} measured from an aircraft, nonunity sea surface emmisivity effects and absorption by the atmospheric layer between the instrument and the sea surface must both be accounted for, while on a ship, the raw subsurface measurement T_m needs to be corrected for the warming of the ocean surface by solar radiation (the "warm layer") and the cooling of the upper few millimeters of the surface due to evaporation, conduction, convection, and irradiance (the "cool skin") [*Fairall et al.*, 1996a].

In addition to determining corrections from specific comparisons, all low-altitude (< 100 m) aircraft irradiance and SST data collected during the IOP were merged and compared with the ship and buoy data for identical time periods. Analysis of this larger data set reveals the nature of the variability of the near-surface radiative fluxes and SST during COARE.

2. Aircraft Instrumentation and Processing

Pyrgeometers, pyranometers, and precision radiation thermometers have been widely used on aircraft for measuring radiative fluxes and SST. These instruments, which are often adapted from ground-based instruments, usually require physically based corrections to compensate for aircraft attitude and elevation, and exposure to environmental changes. Some of the aircraft data-processing methods will be presented here along with problems encountered in the COARE aircraft radiation and SST data set.

2.1. Shortwave Radiation

All five aircraft used Eppley precision spectral pyranometers (PSPs) with clear domes of Schott optical glass (WG295; 0.285-2.8 μm band pass) to measure the downwelling and upwelling shortwave irradiance. For this study we do not consider near-infrared data collected by the WP-3D PSPs with colored glass domes. The calculation of shortwave irradiance from the raw PSP data requires physically based corrections for thermal transients within the PSP, response time relative to the rest of the aircraft instrumentation, and aircraft attitude relative to the Sun position. Since the attitude correction depends on the angle of the direct solar radiation relative to the sensor orientation, it is only applicable to the upward looking PSP.

After deep soundings (i.e., a descent from 5000 m to 30 m in about 20 min) it was observed that the large environmental temperature changes caused the WP-3D PSPs to be out of thermal equilibrium. Since the PSPs were not equipped with temperature sensors, the nearby pyrgeometer case and dome thermistors were used to determine when the PSPs were out of thermal equilibrium. PSP data from these periods were excluded from the study. The pyrgeometers were used because they are similar in exposure and design to the PSPs. More detail about the thermal equilibrium problem is in section 2.2 on pyrgeometers. PSP data from the other aircraft were not obviously affected by thermal transients.

The aircraft-attitude correction to the measured upward looking PSP data is straightforward on clear days but complicated when clouds block the direct component of the incoming solar radiation. The radiative-

transfer model criterion of *Saunders et al.* [1992] was used to distinguish when direct downwelling solar radiation was present. This model expresses the threshold flux value Q_{crit} (in watts per square meter) between direct and diffuse radiation as a function of solar zenith angle (θ, the angle between the Earth's normal and the Sun's rays),

$$Q_{\text{crit}} = 920\ (\cos\theta)^{1.28}. \tag{1}$$

Values above Q_{crit} indicate that direct solar radiation was present, and the aircraft attitude correction was applied to these PSP data. This expression was used for all of the aircraft data except for 340A, whose solar flux data were all treated as direct.

The aircraft-attitude correction to find Q_{SW} has been determined by several investigators [*Saunders et al.*, 1992; *Bannehr and Glover*, 1991] and is given by

$$Q_{\text{SW}} = (Q_{\text{SW}})_m \frac{\cos\theta}{\cos\beta}, \tag{2}$$

where $(Q_{\text{SW}})_m$ is the measured direct solar flux (as determined by (1)), and β is the angle between the Sun's rays and the PSP normal. The angle β is geometrically related to the aircraft attitude angles (pitch P, roll R, and heading H) by

$$\begin{aligned}\cos\beta \;=\; & -\cos R \sin P \sin\theta \cos(H - A) \\ & -\sin R \sin\theta \sin(H - A) \\ & +\cos R \cos P \cos\theta,\end{aligned} \tag{3}$$

where A is the solar azimuth angle, and P, R, and H are measured by the aircraft inertial navigation system (INS). Since the PSPs have a finite response time and typically lag the INS instrumentation by about 1 s [*Saunders et al.*, 1992], the WP-3D and N308D upward looking PSP data correction was improved by advancing the PSP data by 1 s prior to using (3). The response-time correction was not applied to the downward looking PSP data since (2) and (3) were not used with the downward looking data. (As mentioned previously, the downward looking PSP is shaded and therefore does not require an attitude correction.)

The above equations assume that the PSP, INS, and aircraft reference frames are perfectly aligned with each other. Errors in alignment are typically accounted for by small adjustments to P and R. For the WP-3D and N308D data processing, a variance-minimization technique similar to that of *Bannehr and Schwiesow* [1993] was used to determine any alignment errors, but the results were inconsistent from flight to flight (errors ranged between $\pm 2°$ for both pitch and roll), and consistent offsets were not obtained. A technique to find the pitch and roll offsets, which uses a box pattern, is described by *Saunders and Barnes* [1990], but such a pattern was not flown by the WP-3Ds. *Boers et al.* [1998] used a high-altitude flight circle to vary the orientation of the aircraft to the Sun and then looked for modulations in the magnitude of Q_{SW} (after correcting with (2)), which would indicate an error in the alignment of the PSP. A COARE mission when both WP-3Ds flew circle maneuvers was examined and indicated that there were no significant alignment problems with the WP-3D PSPs.

An example of the uncorrected Q_{SW} data, $(Q_{\text{SW}})_{\text{m}}$, and the physically corrected Q_{SW} data for a 300-s comparison leg is shown in Figure 1. The attitude correction to the downwelling Q_{SW} data decreases it by about 25-30 W m^{-2} but does not eliminate the difference between the N308D and the WP-3D data (this discrepancy will be discussed in detail later). Since N42RF was in the lead, the high-frequency attitude corrections are most apparent in the data from N43RF and N308D, which were constantly making small attitude adjustments to maintain course.

The enhancement of downwelling Q_{SW} by cloud reflection of the direct solar radiation is apparent when the aircraft formation flew near small cumulus clouds, particularly around 110 s in Figure 1. The upward looking PRT-5 on N308D can be used to sense when the aircraft are under a warm cloud, and an enhancement of about 50 W m^{-2} in Q_{SW} is evident since the aircraft were heading to the northeast and the Sun was setting to the southwest about 30° above the horizon. Immediately after the enhancement (~130 s) the solar radiation decreases sharply as the cloud blocks the Sun.

Here we note that a PRT determines the radiometric temperature, T_{ir}, using a limited field of view (typically less than 2°) over a narrow wavelength band (~8-14 μm), while a PIR measures Q_{LW} over a broad band (3.5-50 μm) with a hemispherical field of view. Therefore small clouds in Figure 1 are prominent in the upward looking T_{ir} data, but barely discernible from the Q_{LW} data.

2.2. Longwave Radiation

Each aircraft, except for C130, used a pair of Eppley precision infrared radiometers (PIRs), or pyrgeometers, to measure upwelling and downwelling longwave irradiance. The Eppley PIR is similar in design to the Eppley PSP, but the dome material is of silicone and an interference filter is vacuum-deposited on the inside dome surface to exclude shortwave radiation. The transmission cutoff is between 3.0 and 4.0 μm. The C130 used MRF-developed pyrgeometers which have silicone domes similar to the Eppley PIR but are much less sensitive to thermal gradients due to a specially designed thermopile [*Foot*, 1986]. The N308D Eppley PIR specifications are detailed by *Glover and Bannehr* [1993]. A brief description of the WP-3D pyrgeometer data processing technique is given below.

Early studies on the energy balance of an Eppley pyrgeometer [*Albrecht et al.*, 1974; *Albrecht and Cox*, 1977] resulted in the following expression for longwave irradiance:

$$Q_{\text{LW}} = \frac{\Delta V}{Gs} + \epsilon_0 \sigma T_{\text{c}}^4 - B\sigma(T_{\text{d}}^4 - T_{\text{c}}^4), \tag{4}$$

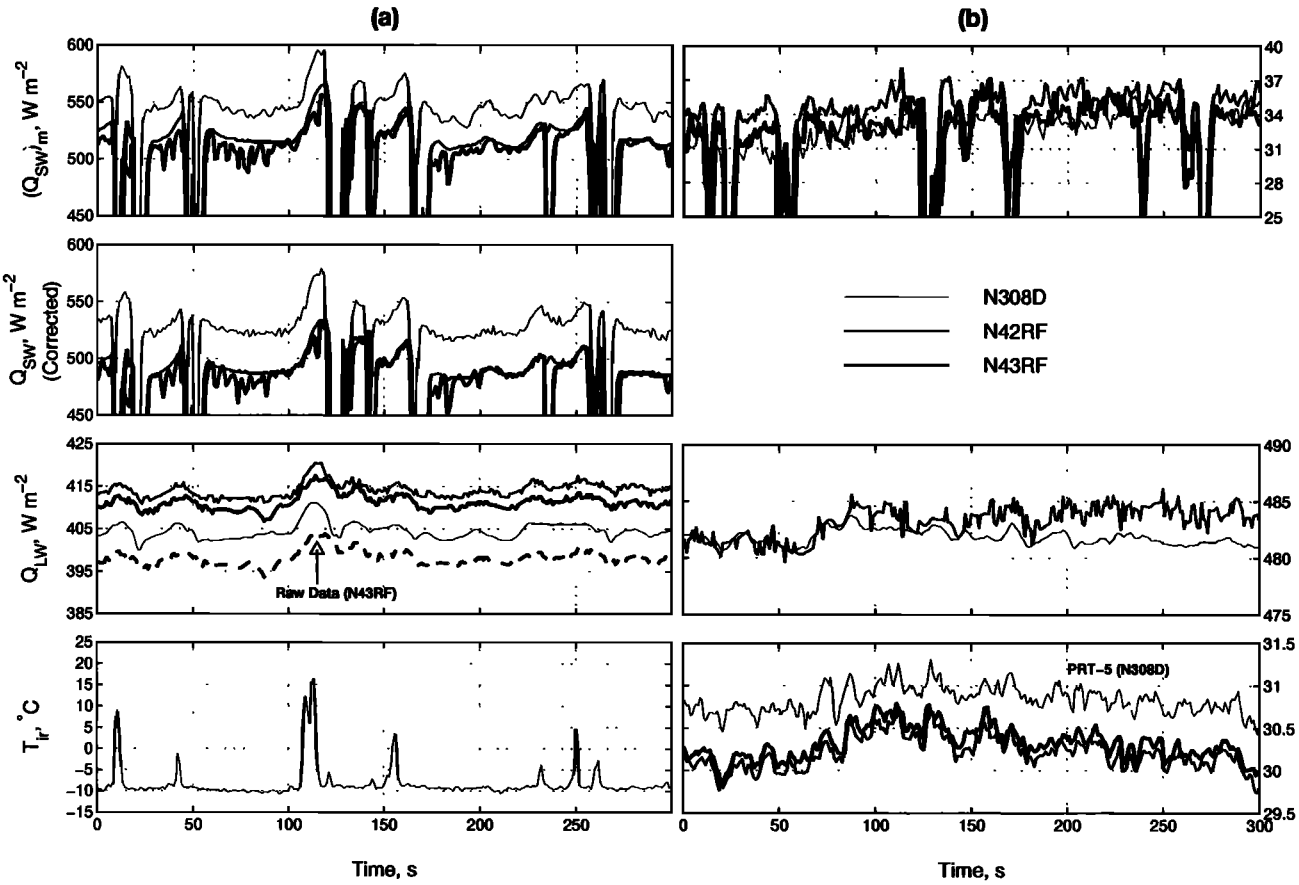

Figure 1. Time series from a three-aircraft comparison leg on 921128 (0506:00 - 0511:00 UTC) of shortwave flux Q_{SW}, longwave flux Q_{LW}, and indicated radiometric temperature T_{ir} measured by (a) upward looking and (b) downward looking instruments. The N308D PRT-5 data are shown. For this run, the mean solar zenith angle is 58.3°, and the solar azimuth is 245.9°. For Q_{LW}, N43RF data are calculated with (solid), and without (dashed), the empirical correction to T_d (explained in the text). No other empirical correction has been applied to any of these data.

where ΔV is the thermopile voltage output; s is the radiometer sensitivity factor; G is the gain factor of the thermopile amplifier (used on the WP-3Ds); ϵ_0 is the emissivity of the thermopile paint; σ is the Stefan-Boltzmann constant; T_d is the dome temperature; T_c is the case temperature; and B is the ratio of the dome emissivity to the transmissivity. Even though analytic expressions exist for s and B, they are usually determined by calibration. An extensive comparison of PIR calibration techniques can be found in the work of *Philipona et al.* [1998].

Recent reexaminations of the basic principles of the Eppley pyrgeometer by *Philipona et al.* [1995] and *Fairall et al.* [1998] identify several problems in the original derivation of (4), such as neglecting one component of the PIR radiation budget (the reflection of thermopile irradiance by the inside of the dome) and inconsistent use of ϵ_0 within the derivation. Another problem with using (4) is that different investigators use different values for ϵ_0.

Fairall et al. [1998] derived two equations to describe the PIR radiative balance, which depend on how the instrument is calibrated. One of these equations is not discussed here since it requires a laboratory method for calibrating an Eppley PIR [*Payne and Anderson,* 1999] where the so-called "fundamental radiometer sensitivity constant" is determined. The equation used for the WP-3D processing is derived for a PIR which has been calibrated using the "Eppley" method, where the Eppley radiometer sensitivity s_e is known. An Eppley type of calibration was performed on the WP-3D PIRs prior to COARE. With knowledge of s_e the longwave irradiance can be described by

$$Q_{LW} = \frac{\Delta V}{G s_e} + \sigma T_c^4 - B\sigma(T_d^4 - T_c^4), \qquad (5)$$

where the terms are as in (4), but now s has been replaced by s_e, and ϵ_0 has been eliminated from the equation; for an exact description of the Eppley calibration method and the difference between s and s_e, see *Fairall et al.* [1998]. For aircraft-mounted PIRs the factor B has historically been determined by either laboratory calibration or from in-flight data [*Albrecht and Cox,* 1977], and values are typically between 2.5 and 4

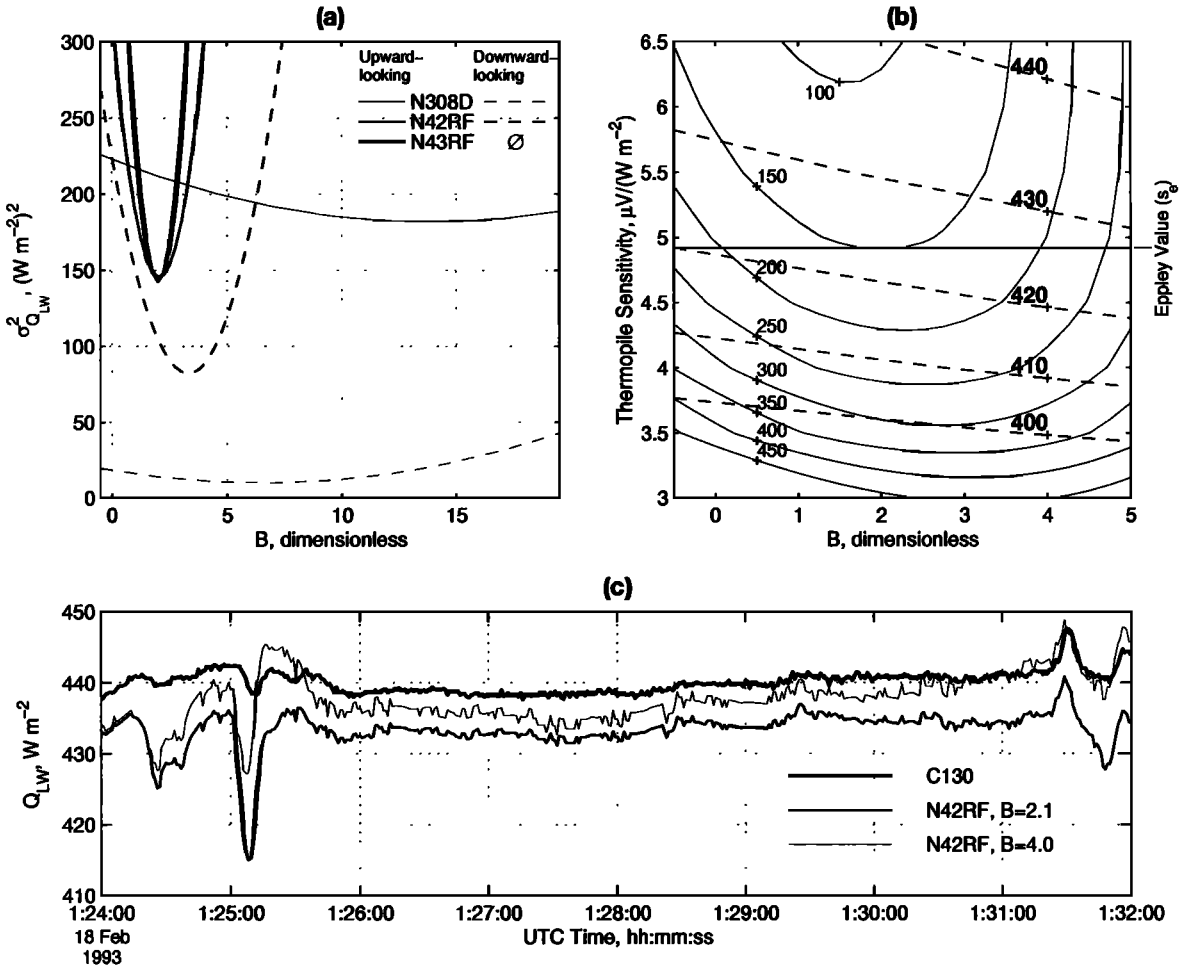

Figure 2. Empirical calibration of the WP-3D pyrgeometers by (a) minimizing the variance of the calculated longwave irradiance Q_{LW} as the calibration coefficient B is varied. (N308D data are included for comparison.) WP-3D calibration results are in Table 2. (b) Contours of the mean (dashed) and variance (solid) of N42RF downwelling Q_{LW} are plotted as the thermopile sensitivity and B are both varied. The Eppley laboratory-determined thermopile sensitivity value s_e is shown as a solid horizontal line. More than 30 hours (about 120,000 1-Hz data samples) of low-level run data were used. Calculated downwelling Q_{LW} time series from a N42RF versus C130 comparison leg is shown in Figure 2c for two different N42RF B values as shown.

[*Fairall et al.*, 1998; *Philipona et al.*, 1998]. *Philipona et al.* [1998] conclude that determination of B is an aspect of PIR measurements which needs further investigation.

For the WP-3D PIR data processing, an empirical variance-minimization method was used to find B. The method uses a large amount of data (all level-run 1-Hz data samples below 500 m from many different missions) and calculates Q_{LW} as B in (5) is varied (s_e is constant; determined by laboratory calibration). Since thermal transients increase the variance of Q_{LW}, and the last term in (5) effectively removes these transients, an optimal B is found by minimizing the variance of Q_{LW}, as shown in Figure 2a. The B values determined with the variance-minimization technique (Table 2) were 2.0 and 2.1 for the N42RF and N43RF upward looking PIRs and 3.3 for the N42RF downward looking PIR (the N43RF downward looking PIR failed). It was encouraging that the optimal B values from the upward looking PIRs on N42RF and N43RF were in close agreement, since the PIR dome material was identical, and these are similar aircraft with similar PIR installations. These values were used in the WP-3D PIR data processing rather than the nominal value of $B = 4$

Table 2. Calibration Coefficients of WP-3D Pyrgeometers

	Upward Looking			Downward Looking		
	s_e	G	B	s_e	G	B
N42RF	4.92	1025.3	2.1	4.15	1029.9	3.3
N43RF	3.98	1060	2.0	4.02	1050	-

Values shown are for the Eppley thermopile sensitivity s_e, the amplifier gain G, and the empirical calibration coefficient B. G and B are dimensionless, and s_e has the units of $\mu V/(W\ m^{-2})$. The N43RF downward looking sensor data were unusable; therefore no B value is included.

primarily based on observations from the comparison time periods. As an example, Figure 2c shows C130 and N42RF Q_{LW} data using two B values for N42RF. The difference between N42RF and C130 data is much more consistent using $B = 2.1$, which indicates that the thermal transients in the N42RF data are being properly eliminated (recall that the C130 PIR is less sensitive to thermal gradients). The 6 W m^{-2} mean difference ($\sim \pm 1\%$) between the N42RF and the C130 Q_{LW} data is further discussed in section 3.1.2.

The same procedure applied to the N308D upward and downward looking PIR data resulted in less distinct variance minima, and therefore the N308D NCAR-processed Q_{LW} data (calculated using (4) with $\epsilon_0 = 0.986$, and $B = 5.5$) were used in this study. Also, in Figure 2a the large difference seen in the minimum of the Q_{LW} variance between the N42RF downward looking sensor and that from N308D was due to extra noise and drift in the N42RF data, which for example can be seen in the time series of Figure 1b. The cause of this noise is unknown and should be removed with a digital low-pass filter.

Since the variance-minimization method assumes the s_e value to be accurate, the nonlinear relationship among Q_{LW}, B, and s_e was further explored in Figure 2b by varying both B and s_e in (5) and examining the mean and variance contours of the calculated N42RF downwelling Q_{LW}. *Fairall et al.* [1998] show that the relative difference between two PIRs can be decreased by making small adjustments to either s_e or B on one of the PIRs (whether to adjust s_e or B depends on if the difference between the sensors shows dependence on thermopile output). While these adjustments do allow for better relative agreement between two PIRs, they are not useful in calibrating a single PIR and give no indication as to which sensor is more accurate. Rather than adjust either B or s_e, we chose the simpler approach of making small empirical corrections to Q_{LW} after comparing Q_{LW} data between the various platforms (see sections 3.1.2 and 4.1). Also, in Figure 2b, observe that if s_e is in error by a small amount (less than 10%), the method will still converge to a similar B value, and the mean of the calculated Q_{LW} will be affected by only a few watts per square meter.

Other problems were encountered with the COARE aircraft PIRs. For N42RF, T_c data from the downward looking pyrgeometer were unusable for the first two flights (921102 and 921106). On N43RF the downward looking thermopile output was not responsive (see Figure 3) throughout the entire IOP, and therefore these

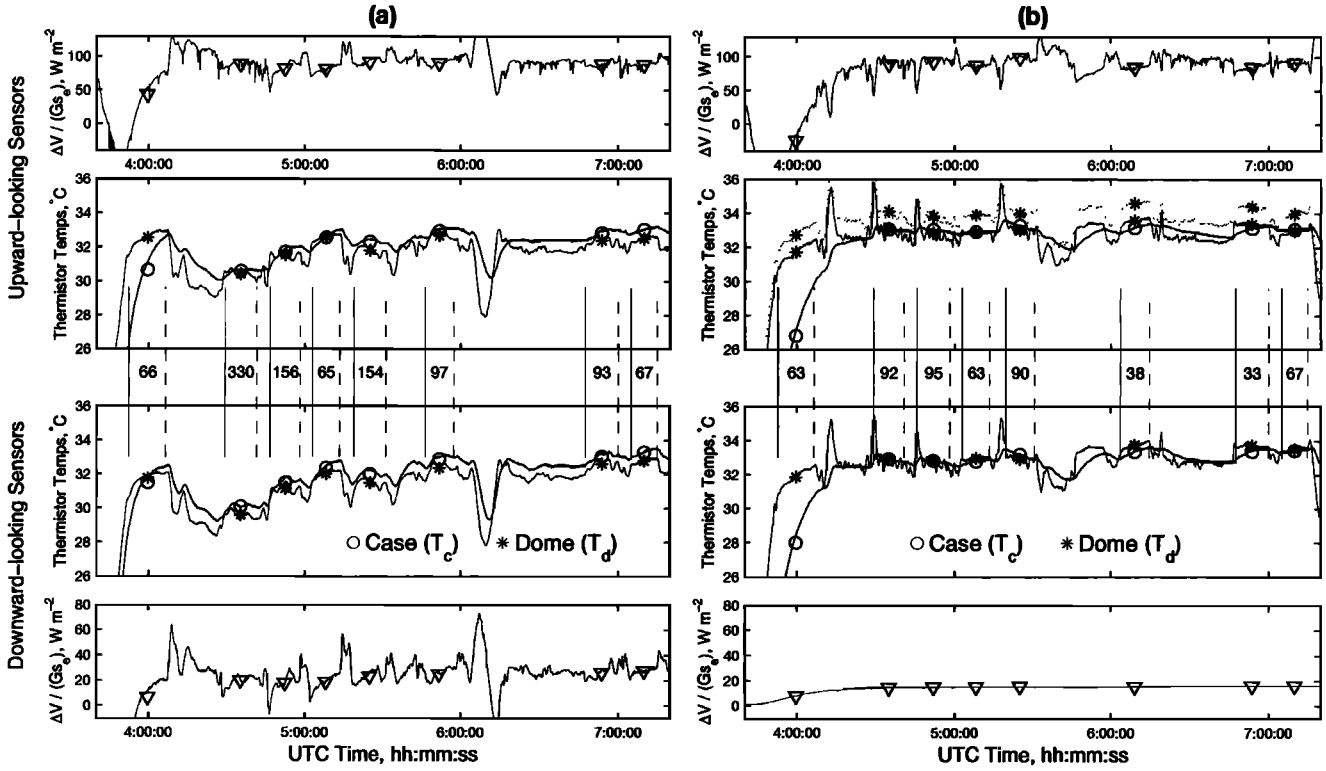

Figure 3. Time series of (a) N42RF and (b) N43RF pyrgeometer data from 921128. Symbols represent level-run mean values, with the mean elevation of the run given between the vertical bars (which indicate the start (solid) and end (dashed) time of the run). Temperature is from the case (T_c) and dome (T_d) thermistors, as indicated. For the N43RF upward looking T_d data there are both raw (dashed) and empirically adjusted (solid) data shown (see text for details). Modulations in the N43RF T_d data are due to variations in N43RF true airspeed. $\Delta V/Gs_e$ is the calibrated thermopile output; for more details see Table 2.

data were rendered useless. The upward looking N43RF thermopile data were contaminated with spikes, which were eliminated by an interpolation scheme as part of the data processing. Also, for N43RF, on 930201 PIR/PSP data were not recorded due to data system problems. The N308D downward looking PIR was not working during flights 921203-921206 and 921209-921214. All WP-3D and N308D PIR data with the above mentioned problems are not included in the comparisons. The downward looking PIR on 340A did not function correctly; therefore the measured surface temperature (discussed in section 2.3) and the Stefan-Boltzmann law were used to estimate the upwelling longwave flux values [*Williams and Hacker,* 1993]. Also, the 340A radiative flux data from the first 340A mission (930109) are excluded from the study due to problems with the PIRs, PSPs, and data-logging equipment.

Another problem with the WP-3D radiation data, previously mentioned in section 2.2 with regard to PSPs, is that thermal gradients in PIR/PSP sensors (due to large, sudden temperature changes) can considerably degrade measurement quality. These time periods mostly occur after ascents or descents. The Eppley PIR thermal recovery time is about 5 min [*Albrecht and Cox,* 1977; *Foot,* 1986]. Since the PIR case T_c and dome T_d thermistors indicate the different response time of the case and dome after sudden temperature changes (the dome being more exposed to the environment than the case), the difference between T_c and T_d was used as an indicator of the degree of thermal equilibrium within the instrument. After examining T_d-T_c data from all low level runs, an estimate of when these instruments were in thermal equilibrium was determined, and time periods when T_d-T_c exceeded a certain criterion were excluded from this study. For example, on N43RF, the PIR and PSP data were used only when the downward looking PIR T_d-T_c difference was between -1.2°C and 1.7°C. (Deciding to use the downward looking PIR was arbitrary.) Figure 3 shows an example of the large difference between T_d and T_c on the first run (at ~ 0400:00 UTC, after descending from 5000 to 100 m) and the relative agreement on all subsequent runs. On the basis of the N43RF criteria the first run would be excluded from our study, while all other runs would be acceptable. If all low-level runs by the WP-3Ds are considered, about 10% of the PIR/PSP data were rejected due to non thermal equilibrium conditions within these instruments. The N308D, C130, and 340A PIR data did not appear to have significant thermal equilibrium problems.

2.3. Radiometric Sea Surface Temperature

Surface temperature measurements were made from the aircraft using narrowband precision radiation thermometers (PRTs) (see Table 1 for details). The optical filters differed slightly between the individual instruments but were all centered about 10 μm. Accuracies from manufacturer's specifications for T_{ir} range from ±0.5 to ±1.0 °C. Calculation of the sea surface skin temperature T_s from the indicated surface temperature T_{ir} requires many additional considerations such as seawater emissivity, surface reflectance, absorption of surface-radiated energy by the intervening atmosphere (primarily by water vapor), emitted energy from the surrounding atmosphere, and the surrounding cloud conditions [*Hignett,* 1998; *Katsaros,* 1980; *Saunders,* 1970, 1967]. The T_{ir} data in the current study are corrected for atmospheric effects (i.e., water vapor absorption) and reflected downwelling longwave radiation (i.e., reflected sky radiance). These corrections result in T_s being greater than T_{ir}. It should be noted that the T_s calculation involves the input of other measured quantities (e.g., radar altitude and Q_{LW}), which if not measured accurately degrade the quality of the T_s data. Surface roughness (i.e., the sea state) is another factor that may affect the radiometric surface readings [*Hagan et al.,* 1997] and may be important when comparing aircraft T_s data with the bulk measurements from the surface platforms.

To account for the emission and absorption of the underlying atmosphere on T_{ir} measurements, data from the N42RF downward looking PRT-5 during level runs from four different mission dates over the altitude range 30 m to 450 m were used (Figure 4). These data indicate an effective T_{ir} change of -0.0017 °C m^{-1} (primarily because of atmospheric absorption) as distance from the surface increases. This value is comparable to the -0.001°C m^{-1} found for a tropical atmosphere with MODTRAN [*Hignett,* 1998] and to the -0.002°C m^{-1} used by *Lambert and Durand* [1998] for a Barnes PRT-5 (8-14 μm). The -0.0017°C m^{-1} correction was applied to data from all five aircraft. Since most of the data used in the present study were obtained below 100 m, the effect of this correction is small.

The radiance measured by a downward looking PRT is composed of two primary components; the emitted energy at the sea surface and the reflection of sky radiance (L_{sky}). The aircraft T_{ir} data were corrected for L_{sky} using a tropical atmosphere model which estimates the empirical relationship between downwelling Q_{LW} and L_{sky} [*Hignett,* 1998]. Appropriate coefficients, based on the optical band-pass filter of each particular PRT were used. The magnitude of this correction depended on cloud conditions and was of the order 0.3-0.5°C, where the larger value corresponds to clear-sky conditions. The L_{sky} correction can be measured directly using an upward looking narrowband infrared thermometer, as was available on N308D [*Liu and Katsaros,* 1984]. (A comparison of N308D T_{ir} data corrected using the PIR versus the upward looking PRT is discussed below.)

A second very high precision radiometer (built at the Jet Propulsion Laboratory (JPL)) which had in-flight changeable filter bandwidths flew on the N308D [*Hagan et al.,* 1997]. During the boundary layer portion of the flight missions the instrument generally operated

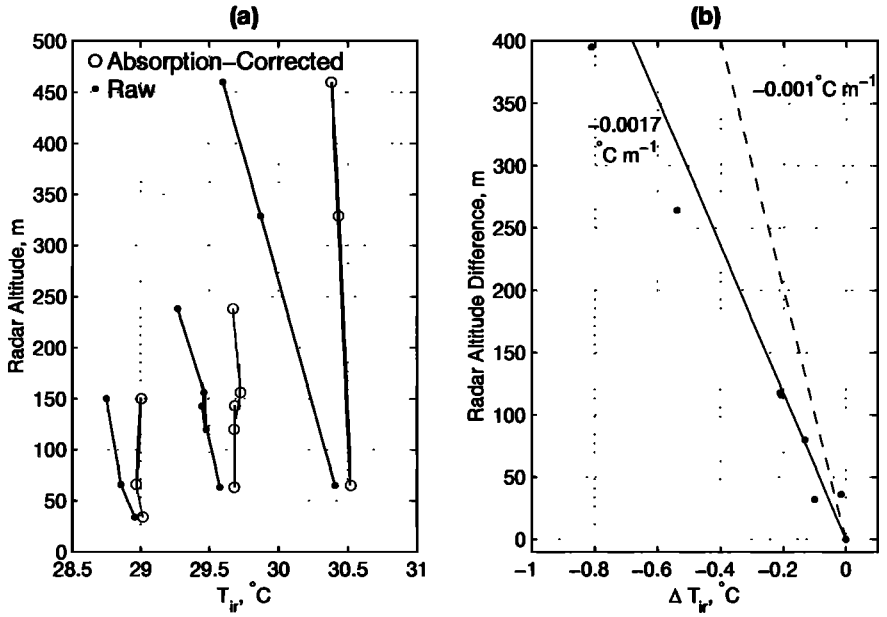

Figure 4. Median level-run values from the N42RF radiometer for (a) raw and absorption-corrected data and (b) differences between these data at various elevations. The level legs are selected from four different missions (921126, 921128, 930117, and 930118) and are from runs where N42RF flew over the same area at different elevations. Each symbol represent the median values from the entire level-leg and the lines in Figure 4b are for an absorption of -0.0017°C m^{-1} (solid) and -0.001°C m^{-1} (dashed).

using an optical filter located between 10 and 11 μm, centered near 10.6 μm. The data from this instrument were corrected for sky reflectance using the upward looking PRT-5 on N308D. The accuracy of these data relative to ship and buoy measurements has been provided elsewhere [*Hagan et al.*, 1997]. However, a subset of measurements is provided here to show the correspondence to the N308D PRT-5 measurements. A comparison of the raw T_{ir} data collected by these two instruments is given in Figure 5a, and it can be observed that the shape of these frequency distributions is somewhat different. After correcting these T_{ir} data to obtain T_s, and applying empirical corrections (explained in section 3.1.3), the variance of the PRT-5 and JPL T_s data distributions are more similar (Figure 5b). Also shown in Figure 5b, using either the upward looking PRT-5 or the PIR to correct T_{ir} for L_{sky} results in similar T_s distributions; however, small-scale differences in features of T_s are present (not shown here) since the pyrgeometer data are hemispherically integrated. Since an upward looking pyrgeometer was used to correct for L_{sky} on the WP-3Ds, C130, and 340A, the PIR-corrected data from N308D are used in this study. It should be noted that the N308D downward looking PRT-5 data some-

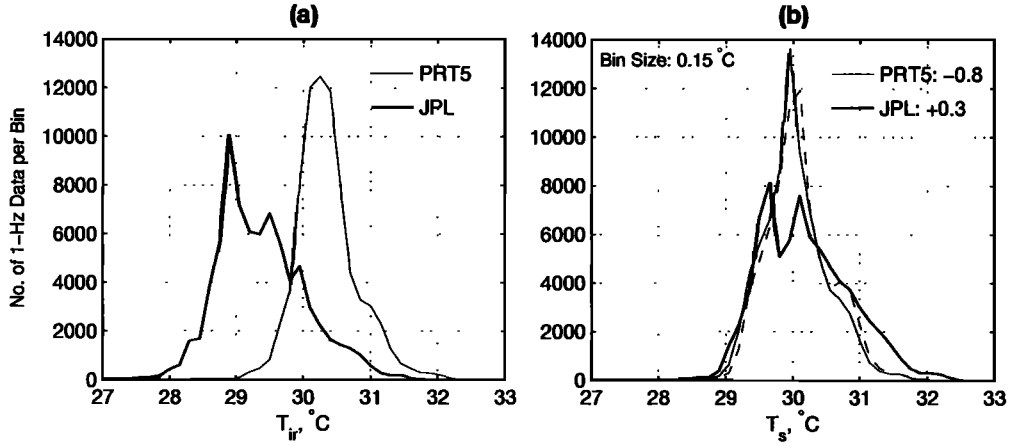

Figure 5. Frequency distributions of N308D (a) indicated surface temperature T_{ir} and (b) sea surface skin temperature T_s, which includes corrections for atmospheric absorption, reflected sky radiance, and empirical corrections (see text for details). These data were obtained from level runs below 500 m. The PRT-5 T_s data in Figure 5b were corrected for sky radiance by using the upward looking PRT-5 (dashed), and the upward looking pyrgeometer (solid).

times contained large transient effects, presumably due to thermal gradients after large altitude changes; more details on this problem are discussed by *Serra* [1996].

3. Aircraft-Aircraft Comparisons

In this section, results from dedicated aircraft "wingtip-to-wingtip" comparison time periods are presented which lead to proposed empirical corrections to some of the aircraft data. In addition, statistics of data from each aircraft for all TOGA COARE low-level runs are compared. This provides a broader range of data than was obtained in the dedicated comparisons (since these comparisons were not performed for every mission, and certain aircraft combinations did not compare with each other) and also provides further insight into the data and proposed corrections.

3.1. Wingtip-to-Wingtip Comparisons

A wingtip-to-wingtip comparison period is defined as the time interval when two or three aircraft are flying below 250 m on a constant heading with small lateral (< 100 m), longitudinal (< 100 m), and vertical (< 10 m) separations. There were a total of 38 time periods that ranged from 30 s (approximately 3 km) to over 20 min (approximately 120 km) and satisfied the above conditions. Because of instrumentation difficulties (explained previously), some parameters have more comparison data than others (see Table 3).

Comparison results are based on 100-s (approximately 10 km) means of 1-Hz aircraft data and displayed with both scatter and box-and-whisker plots. A box plot displays data in quartiles where the "box" indicates the interquartile range (iqr) over which the middle 50% of the data are distributed, the lowest 25% of the data are between the lower end of the box and the lowest whisker end point, and the upper 25% are between the top of the box and the upper whisker. The line through the box shows the median. The mean is designated by a "plus" and outliers (defined as points that are greater than 1.5 × iqr away from the edge of the box) by a "circle". For comparison legs less than 100 s, leg-long statistics are used. For more details on the comparison techniques, see *Burns et al.* [1999].

For the five COARE aircraft, there were, as shown in Table 3, only five different combinations of these aircraft that flew comparisons (since C130 compared only with N42RF and 340A only with N308D). For this reason, N42RF and N308D are considered "reference" aircraft against which the other aircraft are compared. The various aircraft combinations (along with the number of 100-s segments for each combination) and the corresponding plotting symbols are shown in Table 3.

3.1.1. Shortwave radiation. After applying the physical corrections to calculate downwelling Q_{SW}, and neglecting the data out of thermal equilibrium, the results from all wingtip-to-wingtip comparison legs are shown in Figures 6a1-6a2. From the box plots of these comparison data (Figure 6a2) it is clear that the N308D Q_{SW} data were greater than those of the other aircraft. To adjust for this difference, the N308D data were reduced by 6%. Results with the empirically corrected N308D data are shown in Figures 7a1-7a2 and lead to an estimate of data accuracy of 3±16 W m^{-2} (~ ±2%). (The method to calculate these statistics is described in the conclusions.) For the upwelling Q_{SW} measurements, there were no empirical corrections applied, and the agreement is about 3±4 W m^{-2}, which is a significant percentage of the observed range (~ ±8%).

3.1.2. Longwave radiation. The method to calculate the longwave irradiance from the measured data is detailed in section 2.2. Examination of T_d and T_c data from the WP-3D and N308D pyrgeometers revealed that the T_d-T_c difference from the N43RF upward looking PIR was inconsistent with those from the other PIRs (see Figure 3). This large bias between T_d

Table 3. Number of Aircraft Wingtip-to-Wingtip and Aircraft-to-Surface Platforms TOGA COARE Comparison Periods

		Aircraft-to-Surface Platform						
Wingtip-to-Wingtip Combinations	No.[a]	Aircraft	IMET No.[b]	ATLS No.[b]	WECM No.[b]	WAVE No.[b]	FRNK No[b]	Symbol Legend
N43RF, N42RF[c]	118	N42RF	36	6	8	26	6	△
C130, N42RF[c]	34	C130	4	2	0	0	2	●
N308D, N42RF[c]	59	N308D	15	8	5	11	30	□
N43RF, N308D[c]	71	N43RF	21	4	6	23	10	▽
340A, N308D[c]	6	340A	5	2	6	3	28	○

Column 9 is the symbol legend to be used in Figures 6-8, 11, and 13-16.

[a]Number of 100-s mean values from the 38 aircraft wingtip-to-wingtip comparisons. Values shown are for SST comparisons; other parameters may have slightly fewer comparison points (due to instrumentation failures). See text for details.

[b]Number of aircraft runs over surface platforms.

[c]Aircraft designated as the "reference" during wingtip-to-wingtip comparisons.

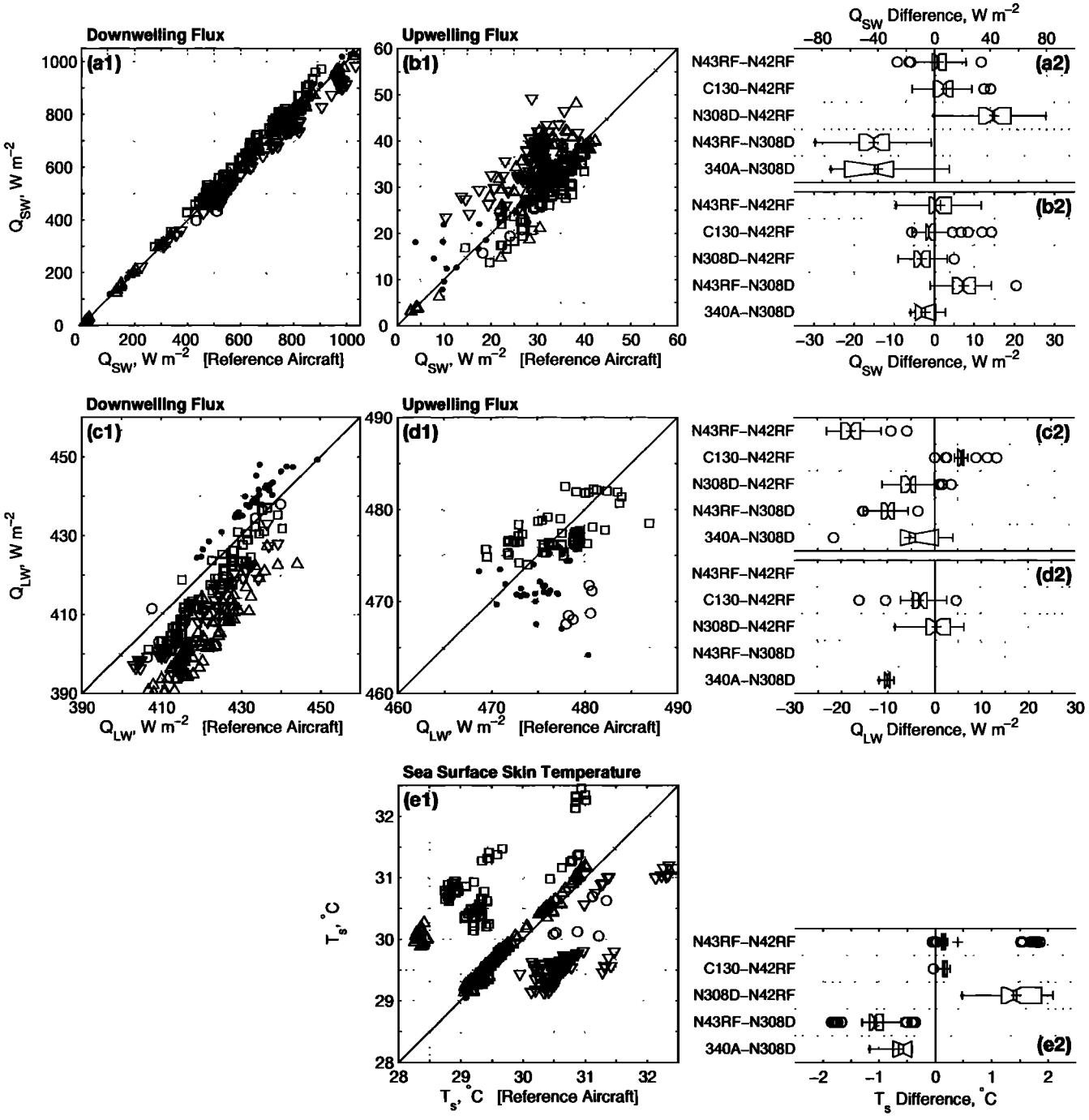

Figure 6. Scatterplots and box plots comparing downwelling (a1-a2) and upwelling (b1-b2) shortwave irradiance Q_{SW}, downwelling (c1-c2) and upwelling (d1-d2) longwave irradiance Q_{LW}, and sea surface temperature (e1-e2) T_s. Symbols and the "reference" aircraft for each pair are shown in Table 3. No N43RF upwelling Q_{LW} data were calculated due to instrumentation problems.

and T_c significantly decreased the calculated mean value of Q_{LW} using (4), as shown in the time series of Figure 1 (dashed line). As a remedy for this situation, T_d from N43RF was empirically decreased by 1.0°C which resulted in better agreement between T_d and T_c (Figure 3b, the second panel), and the calculated Q_{LW} data were brought closer to those of the other aircraft (Figure 1). On an aircraft, where dynamic heating of the dome may be present, improper placement of the dome thermistor may result in a consistent measurement bias. As an indication of how susceptible PIR domes are to temperature gradients, *Philipona et al.* [1995] observed dome temperature gradients of over 0.3°C with ground-based PIRs and suggested using three thermistors at a 45° elevation to properly characterize the dome temperature (for the WP-3D PIRs, only a single thermistor

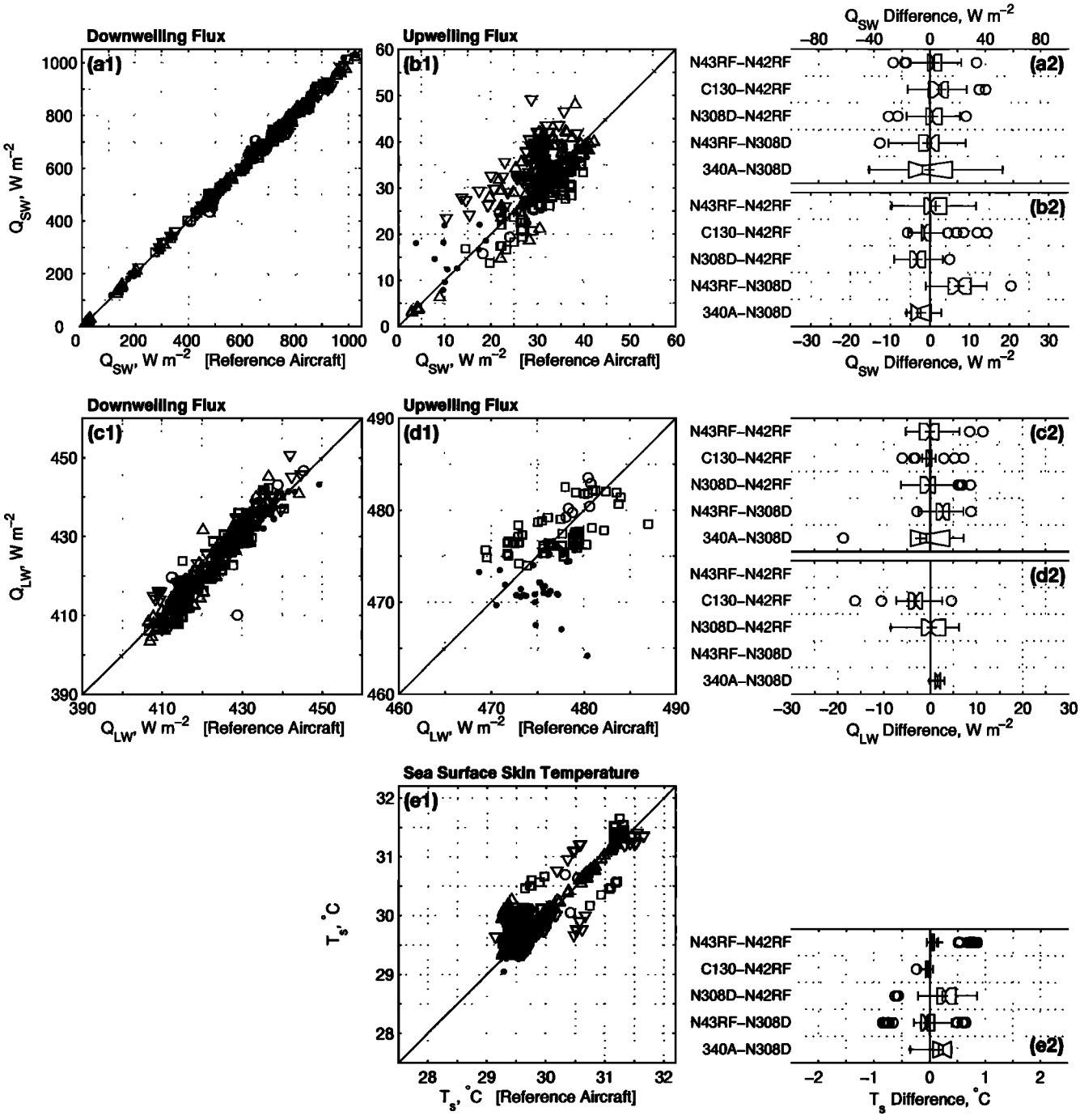

Figure 7. As in Figure 6 but with empirical corrections included.

was used). *Payne and Anderson* [1999] found that PIR thermistor accuracy can also be degraded if the manufacturer's nominal calibration is used instead of laboratory calibrations. It should be noted that decreasing T_d by 1.0°C affected the mean value of Q_{LW} but not the empirically determined B value (as described in section 2.2).

As mentioned previously, the 340A upwelling Q_{LW} data were not measured directly with an Eppley PIR since the instrument malfunctioned. For 340A, upwelling Q_{LW} was estimated using T_s and the Stefan-Boltzmann law and then low-pass-filtered to simulate the averaging of the broadband hemispherical PIR. This technique underestimated the actual flux value due to the difference in viewing angle between the PRT and the PIR and also to the reflected sky radiance (which is removed to calculate T_s) not being included in the calculation. On the basis of the comparisons between 340A and the other aircraft, these two effects were corrected for by increasing the 340A Q_{LW} data by 2.5%.

Comparisons of downwelling longwave irradiance data (with no empirical corrections) from all wingtip-to-

wingtip legs are shown in Figure 6. After applying the empirical correction to the upward looking N43RF T_d data (explained above) and making small corrections to Q_{LW} from C130 (decreased by 1.3%), N308D (increased by 1%), N43RF (increased by 1%), and 340A (increased by 2%), the final Q_{LW} values (Figures 7c1-7c2) are in reasonable agreement. The magnitude of these corrections was determined on the basis of consideration of the aircraft-surface platform comparisons (section 4.2) and assuming N42RF data were accurate. For upwelling Q_{LW}, the 340A data were increased by 2.5% to agree with the other aircraft (Figures 7d1-7d2). Note that the number of these comparisons was diminished due to the malfunction of the N43RF downward looking PIR. A complete summary of the empirical corrections is given in Table 4.

After applying the empirical corrections, the upwelling and downwelling Q_{LW} measurements among the aircraft agree to within 1±4 W m^{-2} and 2±3 W m^{-2} ($\sim \pm 1\%$), respectively, which is near the accuracy specifications of the PIRs.

3.1.3. Radiometric sea surface temperature. Data from in-formation flight legs were used to establish empirical corrections to the aircraft T_s data. These necessarily involved some assumptions and judgments, particularly since some instruments had different laboratory prefield and postfield calibrations and showed signs of calibration drift during the IOP. The C130 was equipped with a blackbody target of known temperature which was swung into the field of view of the PRT-4 after each run to provide an *in situ* calibration; therefore C130 data were considered the most accurate among the aircraft radiometers. The C130 compared only with N42RF in the second half of the IOP, and these flights indicated that the N42RF data were low by 0.3°C; other comparisons and the postfield phase laboratory calibration indicated that the empirical correction for N42RF was variable and therefore a flight-date-dependent correction was determined. N42RF and N43RF compared numerous times throughout the IOP, and a correction of 0° to 0.2°C was determined for N43RF. On the basis of comparisons with the R/V *Franklin* (discussed later) and ensemble frequency distributions shown in the section 3.2, the T_s data of the 340A were not empirically corrected. The N308D PRT-5 T_s data were consistently greater than those from the other aircraft (Figure 6) and are therefore empirically reduced by 0.8°C. The J-PL data were corrected by +0.3°C to agree better with the N308D PRT-5 data and those from the other aircraft. A summary of all empirical corrections for T_s is shown in Figure 8 (also see Table 4). After these empirical corrections were applied to the data, the resulting differences among the aircraft were decreased from about 0.7±0.4°C (Figure 6) to 0.1±0.3°C (Figure 7).

3.2. Ensemble Comparisons

After determining empirical corrections from the wingtip-to-wingtip comparison periods, ensemble frequency distributions of all the level-run data collected by each individual aircraft below 100-m elevation were examined. Distributions of the location and elevation of where these data were collected are given by *Burns et al.* [1999, Figure 18]. Figure 9 shows the distributions of Q_{SW}, Q_{LW}, and T_s measured by each of the five aircraft without any empirical correction (but including the "physical" corrections described in sections 2.1, 2.2, and 2.3). When examining these distributions, it is important to realize that even though these data were collected over many different dates and condition-

Table 4. Empirical Corrections to Aircraft and Surface Platform Measurements

		Formula: $X_{adjusted} = X_{original}$ + empirical correction, or $X_{adjusted}$ is corrected by the percentage shown.								
Parameter		C130	N308D	340A	N42RF	N43RF	IMET[a]	WECM[a]	WAVE[a]	FRNK[a]
Q_{SW}, (W m^{-2})	downwelling	0	-6%	0	0	0	0	0	0	0
	upwelling	0	0	0	0	0	0	0	0	0
Q_{LW}, (W m^{-2})	downwelling	-1.3%	+1%	+2%	0	+1%	+7	+8	+7	0
	upwelling	0	0	+2.5%	0	0	0	0	0	0
T_s, (°C)		0	-0.8, +0.3 (JPL)	0	+0.2 to +1.0	0 to +0.2	0	0	0	0

Values shown are for shortwave irradiance Q_{SW}, longwave irradiance Q_{LW}, and sea surface skin temperature T_s. Date-dependent corrections show the minimum and maximum correction values; see Figure 8 for more information.

[a]Surface platform corrections shown here are applied to the data obtained for this study (see *Burns et al.* [1999] for more information). These corrections are in addition to other corrections that may have been applied by the data-processing group. (See documentation with these data for more information about other corrections.)

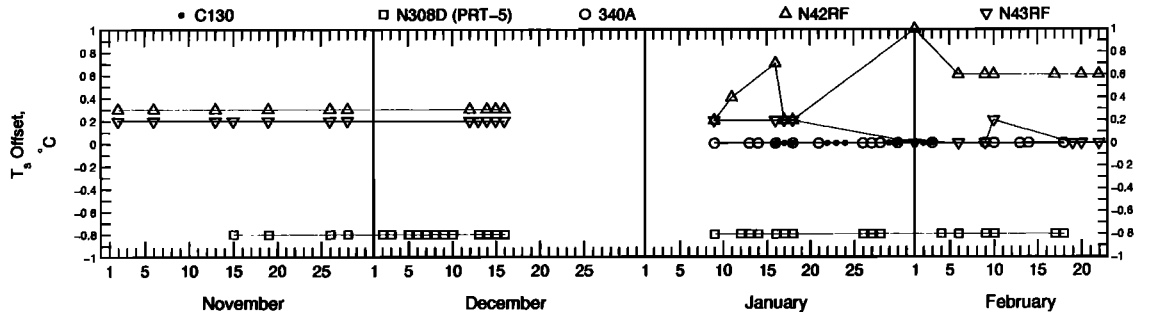

Figure 8. Empirical corrections to adjust aircraft sea surface temperature T_s data. Use legend to identify aircraft. Correction values are shown for each mission flight date. The nominal correction values, in degrees Celsius, are C130 (0), N308D (PRT-5: -0.8, JPL: +0.3), 340A (0), N42RF (+0.2 to +1.0), and N43RF (0 to +0.2).

s, they include many multi-aircraft missions, so similar ranges for the frequency distributions are expected.

Because of the uniform nature of the Q_{SW} distribution, it is difficult to make definitive conclusions about differences between the aircraft from Figure 9a. Recall that from the wingtip-to-wingtip comparisons the N308D Q_{SW} data were found to be too large and therefore were reduced by 6%. Figure 10a shows the same distribution as Figure 9a but for the empirically reduced N308D downwelling Q_{SW} data. One effect of the correction was to shift the upper peak of the N308D data from being above 1000 W m^{-2} to just below 1000 W m^{-2} and thus coincide with the N43RF and C130 largest values.

The downwelling Q_{LW} data distributions without empirical corrections from N42RF and C130 shown in Figure 9b were about 10-20 W m^{-2} greater than those measured by the other three aircraft. Empirical reduction of T_d on N43RF, and applying the previously described small empirical corrections factors (see section 3.1.2), improved Q_{LW} agreement between the aircraft (Figure 10b).

For the upwelling Q_{LW} data, the discrepancy in the 340A Q_{LW} data compared with those from the other aircraft is clear (Figure 9b). As mentioned previously, the 340A data were empirically increased by a factor of 2.5% to agree with the other aircraft, and the resulting distribution can be seen in Figure 10b.

Figure 9c shows the significant differences between the WP-3Ds and the N308D (PRT-5) T_s data frequency distributions (prior to any empirical corrections but including physical corrections). In the gap between these distributions are the C130 and 340A data. Since the C130 data are believed to be of high quality, the N308D data were slightly decreased, and the WP-3D data were slightly increased (details on the empirical corrections are in section 3.1.3) to agree with C130 T_s data. The

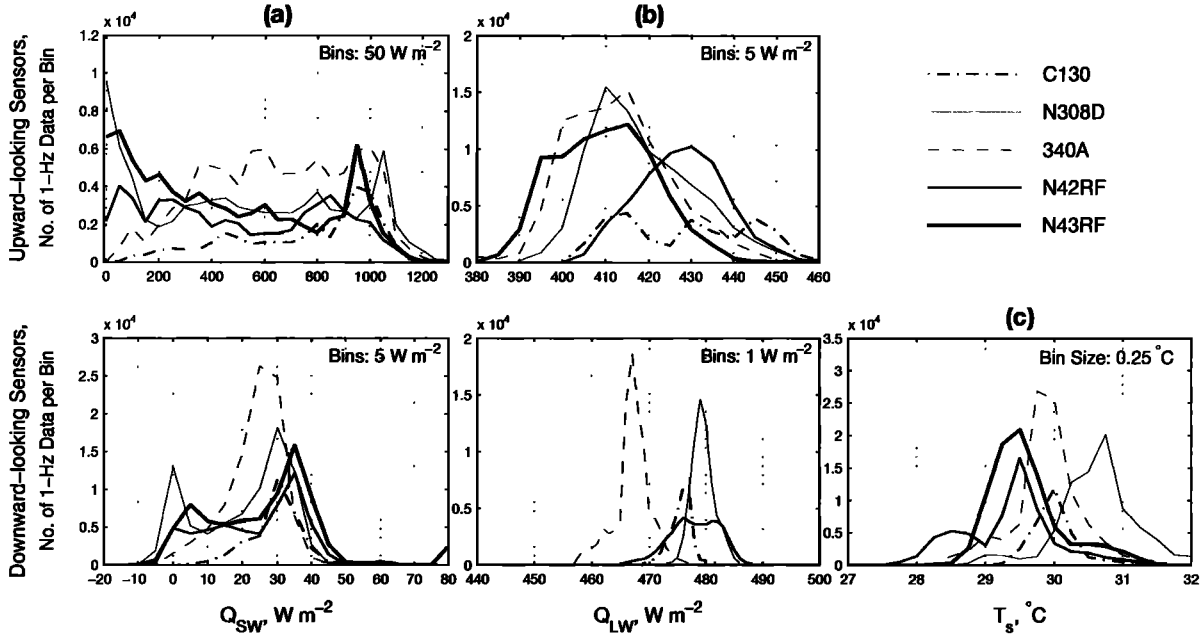

Figure 9. Frequency distributions of (a) shortwave irradiance Q_{SW}, (b) longwave irradiance Q_{LW}, and (c) sea surface skin temperature T_s for low-level runs. Bin sizes are shown in each panel. Aircraft legend is in the top right corner. There are no N43RF upwelling Q_{LW} data due to instrumentation failure.

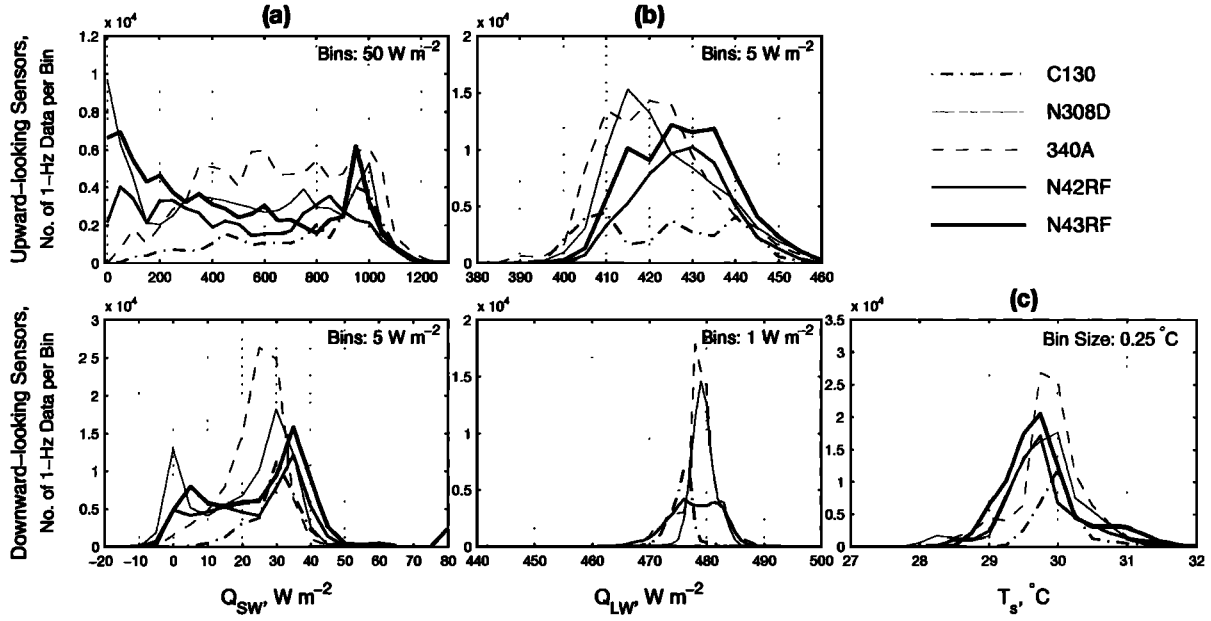

Figure 10. As in Figure 9 except that empirical corrections are included with the aircraft data.

frequency distributions for WP-3D and N308D empirically corrected T_s data are shown in Figure 10c and are in reasonable agreement.

4. Aircraft-Buoy and Aircraft-Ship Comparisons

Dedicated aircraft-buoy and aircraft-ship comparisons were carried out on many of the boundary-layer missions during the IOP. Table 1 provides a summary of the surface platforms considered herein. The technique used to select the ship and buoy overflights within a 15-km radius of a surface platform and below 100-m altitude is described by *Burns et al.* [1999]. A total of 267 such overflights were identified, and a breakdown by platform is shown in Table 3. After applying corrections to the surface-platform data (only summarized here), *Weller and Anderson* [1996] show good agreement in Q_{SW}, Q_{LW}, and SST among the WHOI mooring (hereafter, called IMET), R/V *Moana Wave*, and R/V *Wecoma* over the duration of the three ship-legs near IMET (the three ship-legs were 19, 23, and 7 days long, respectively). Unless stated otherwise, the aircraft Q_{SW}, Q_{LW} and SST data used here include all physical and empirical corrections detailed in the previous sections. It should be noted that since the release of the final, public-domain surface-platform data sets, there has been a reevaluation of the longwave radiation measured from the surface platforms. Some historical details of this reevaluation can be found in the work of *Bradley and Weller* [1997], and the final conclusions are summarized below.

4.1. Shortwave Radiation

All of the surface platforms except for the ATLAS mooring, which did not measure any radiative fluxes, used Eppley precision spectral pyranometers (PSPs) to measure the downwelling shortwave irradiance (see Table 1).

On the basis of a post-COARE comparison of the surface-platform Eppley PSP sensors, the shortwave radiation measurements from *Wecoma* were deemed to be most accurate and used to adjust Q_{SW} data from the other surface platforms. From IMET the Q_{SW} data from the two PSPs deployed were reduced by 3% (first PSP deployed) and 8% (second PSP deployed) [*Weller and Anderson,* 1996]. The *Moana Wave* and *Franklin* Q_{SW} data were increased by 3% and 0.2%, respectively.

The surface platform and aircraft shortwave radiative fluxes were only compared when the fluxes measured by both platforms were above the direct solar flux cutoff criterion described in section 2.1 (see equation (1)). This reduced the possibility of the aircraft being under a cloud while the surface platform was in direct sunlight, and vice versa. Though this restriction reduced the number of comparisons by nearly 50%, it was considered justified since most of the points eliminated were those that revealed large differences. (The standard deviation of the surface platform to aircraft difference was reduced from over 120 W m^{-2} (no data restriction) to about 35 W m^{-2} (restricted data).) Figure 11 shows the agreement between the surface platforms and the aircraft using the restricted data. Almost all differences are between ±50 W m^{-2}.

To supply a summary of the results and assess the effect of the empirical correction to N308D data (Table 4), overall box plots of the ship-aircraft and buoy-aircraft Q_{SW} differences with (bottom box plot) and without (top box plot) the N308D empirical correction are shown in Figure 12b.

4.2. Longwave Radiation

Similar to the shortwave measurements, all the surface platforms except for ATLAS used Eppley precision

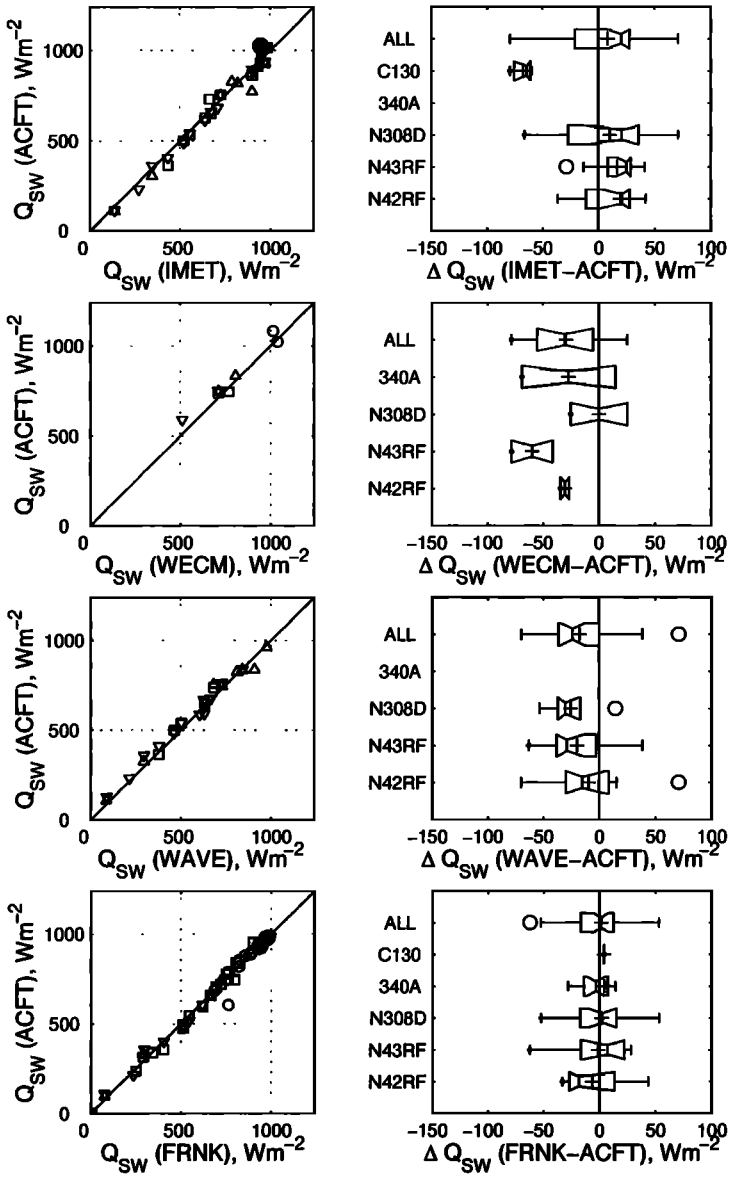

Figure 11. Comparison of downwelling shortwave irradiance measured from aircraft and from IMET (row 1), *Wecoma* (row 2), *Moana Wave* (row 3) and *Franklin* (row 4). Box plots (right-hand column) show the differences between the corrected aircraft measurements and the surface-platform measurements. The solid line is the one-to-one line. Refer to Table 3 for key to symbols.

infrared radiometers (PIRs) to measure the downwelling longwave irradiance (see Table 1).

As described by *Fairall et al.* [1998], longwave irradiance may be calculated from pyrgeometer signals using (5) or, less accurately, by internal compensation for the second term on the right-hand side of (5) with removal of the solar heating error (third term) following the method of *Alados-Arboledas et al.* [1988]. Only the *Moana Wave* recorded all data to properly use (5), so pyrgeometers on *Wecoma* and *Franklin* had biases removed by reference to the *Moana Wave* instrument and applied the Alados-Arboledas correction.

The IMET PIR data from the second deployment had a linear trend removed, the dome-heating correction applied, and then a 12 W m^{-2} bias correction subtracted (incorrectly given by *Weller and Anderson* [1996] as 7 W m^{-2}) based on preliminary intercomparisons with the *Moana Wave* data. Subsequent PIR evaluation by *Fairall et al.* [1998] led to an increase of the *Moana Wave* longwave data by about 7 W m^{-2}. For the present study therefore the archived IMET data have also been increased by 7 W m^{-2} to keep in agreement with the reevaluated *Moana Wave* data. Also for the present study, the archived *Wecoma* data were increased by 8 W m^{-2}, which resulted in better agreement with the other surface-platform Q_{LW} data. The archived *Franklin* data did not require any further adjustment. A summary of additional empirical corrections applied to the surface platform data is given in Table 4. The increase of the surface-platform Q_{LW} da-

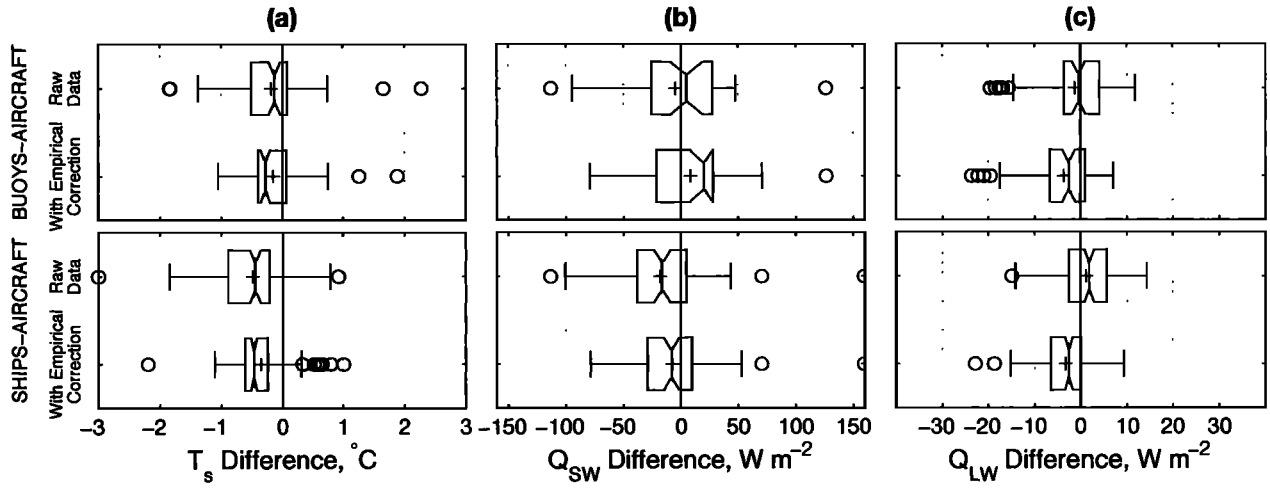

Figure 12. Box plots of mean differences between ship-aircraft and buoy-aircraft measurements of (a) air-sea interface temperature T_s, (b) downwelling shortwave irradiance Q_{SW}, and (c) downwelling longwave irradiance Q_{LW}. Individual platform data are combined on the basis of platform type to form the aircraft, ship, and buoy data sets. Differences are shown with and without the aircraft empirical corrections; for the surface platforms, T_s is calculated from T_m as described in section 4.3; N308D data are from the PRT-5.

ta results in better agreement with measurements made by the R/V *Kexue 1* during COARE [*Song and Friehe*, 1997].

Reasonable agreement and consistent differences were found between the aircraft and the surface platform Q_{LW} measurements (Figure 13). To supply a summary of the results described above and to assess the effect of the empirical corrections on these comparisons, overall box plots of the ship-aircraft and buoy-aircraft Q_{LW} differences are shown in Figure 12c. Though applying the empirical corrections to the aircraft data does not appear to improve the agreement between the aircraft and the surface platforms, the spread in these data is actually decreased (i.e., the length of the box is shorter). For Q_{LW} the magnitude of the empirical corrections to the aircraft data was determined more on the basis of the aircraft wingtip-to-wingtip comparisons than on the aircraft-to-surface platform comparisons.

4.3. Sea Surface Temperature

From the subsurface sea temperature measurements T_m, estimates of the sea surface skin temperature T_s were calculated using the cool-skin and warm-layer components of the COARE bulk algorithm [*Fairall et al.*, 1996b]. The depth of each temperature sensor used in the present study is given in Table 1.

Since the *Moana Wave* floating sensor was so near the surface (5 cm was the nominal depth), only the cool-skin correction was applied in the bulk algorithm to find T_s (i.e., the warm-layer correction was not needed). For *Wecoma*, bucket thermometer readings taken every hour by the watch standers were interpolated to 30-min values and then used as the T_m input to the bulk algorithm. The *Wecoma* SeaBird sensor did not work for half of the first leg and all of the third leg, so these data were not used. For the IMET thermistor at 45 cm depth, both the cool-skin and the warm-layer corrections were applied to find T_s. The ATLAS T_m data were used at the measurement depth of the sensor.

Franklin had a thermosalinograph to measure T_m and an infrared radiometer for the direct measurement of T_{ir} [*Coppin et al.*, 1991]; as archived, the skin temperature estimated from T_{ir} included the addition of a constant 0.4°C to the raw T_{ir} data which corrects for reflection of downwelling sky radiation and the emissivity of the sea surface. In practice, this correction varies depending on viewing angle and sky condition, but 0.4°C is an average value based on samples with the radiometer pointing skyward. The radiometer was not operational the entire IOP, so T_s calculated from the thermosalinograph T_m data was used in this study. Though the depth of the thermosalinograph input was at 2.4 m, the water entering the portal had actually originated from closer to the surface, and a nominal depth of 1 m was used as input to the bulk algorithm to calculate T_s.

The effect of the empirical corrections obtained from the wingtip-to-wingtip comparisons (Figure 8) on the comparisons to the platform T_s data are shown in Figure 14 (without aircraft empirical corrections, column 1; with aircraft empirical corrections, column 2). Note that aircraft data from both columns have been corrected for atmospheric absorption and sky radiance reflection. Overall, the agreement between the aircraft and surface-platform data was improved with empirical corrections applied to the aircraft data (Figure 12c), however the aircraft T_s data are generally greater (0.2°-0.5°C) than those from the surface platforms. The effect of the aircraft T_s empirical offsets is more apparent on ship-aircraft comparisons where the spread has been reduced more than the buoy-aircraft differences.

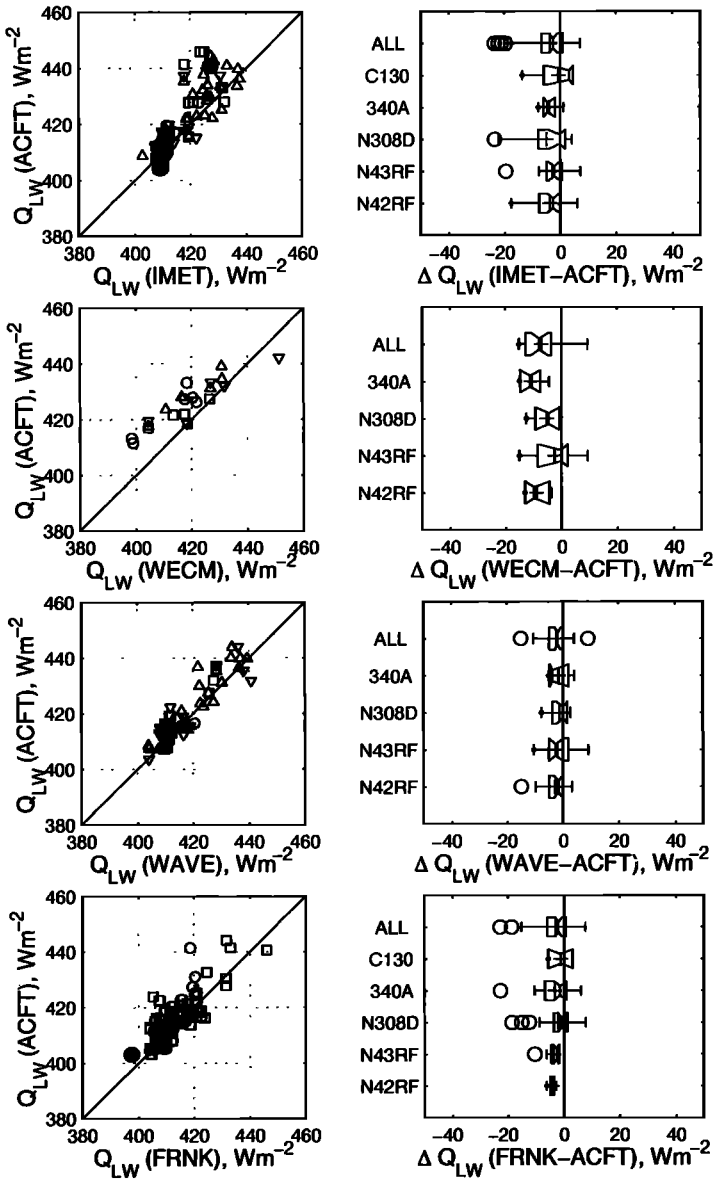

Figure 13. As in Figure 11 except that downwelling longwave irradiance is compared here.

5. Single Mission and Overall IOP Comparisons

Statistics and frequency distributions of the radiation data collected by the various platforms over the entire IOP are compared. Also, time series from single missions and from the entire IOP are considered. Unless otherwise indicated, the comparison techniques used in this section are identical to those of *Burns et al.* [1999].

5.1. Mission-by-Mission Comparisons

Radiative fluxes and SST time series from two 4-hour missions with the previously described physically based and empirical corrections applied are shown in Figures 15 and 16. From these figures, the previously mentioned thermal gradient problem with the WP-3D PSPs/PIRs and N308D PRT-5 can be observed. This problem is most noticeable in Figure 15, where the agreement between the aircraft on the first run (which was a three-aircraft wingtip-to-wingtip comparison leg) was less than that of subsequent runs. Also notice the large spread in the aircraft T_{ir} data compared to T_s data which includes both physical and empirical corrections. Even though conditions were much more variable on 930118 than 921128, data differences between the various platforms were still reasonable. The *Franklin* radiometer was not working on 930118.

As a summary of each IOP mission, the complete 4-month time series of Q_{SW}, Q_{LW}, and SST are plotted in Figure 17, where the surface platform values were averaged over the daylight hours (~12 hours). At first glance it may appear that there were large differences between the surface and the aircraft downwelling Q_{SW} data (Figure 17a2); however, these differences were real,

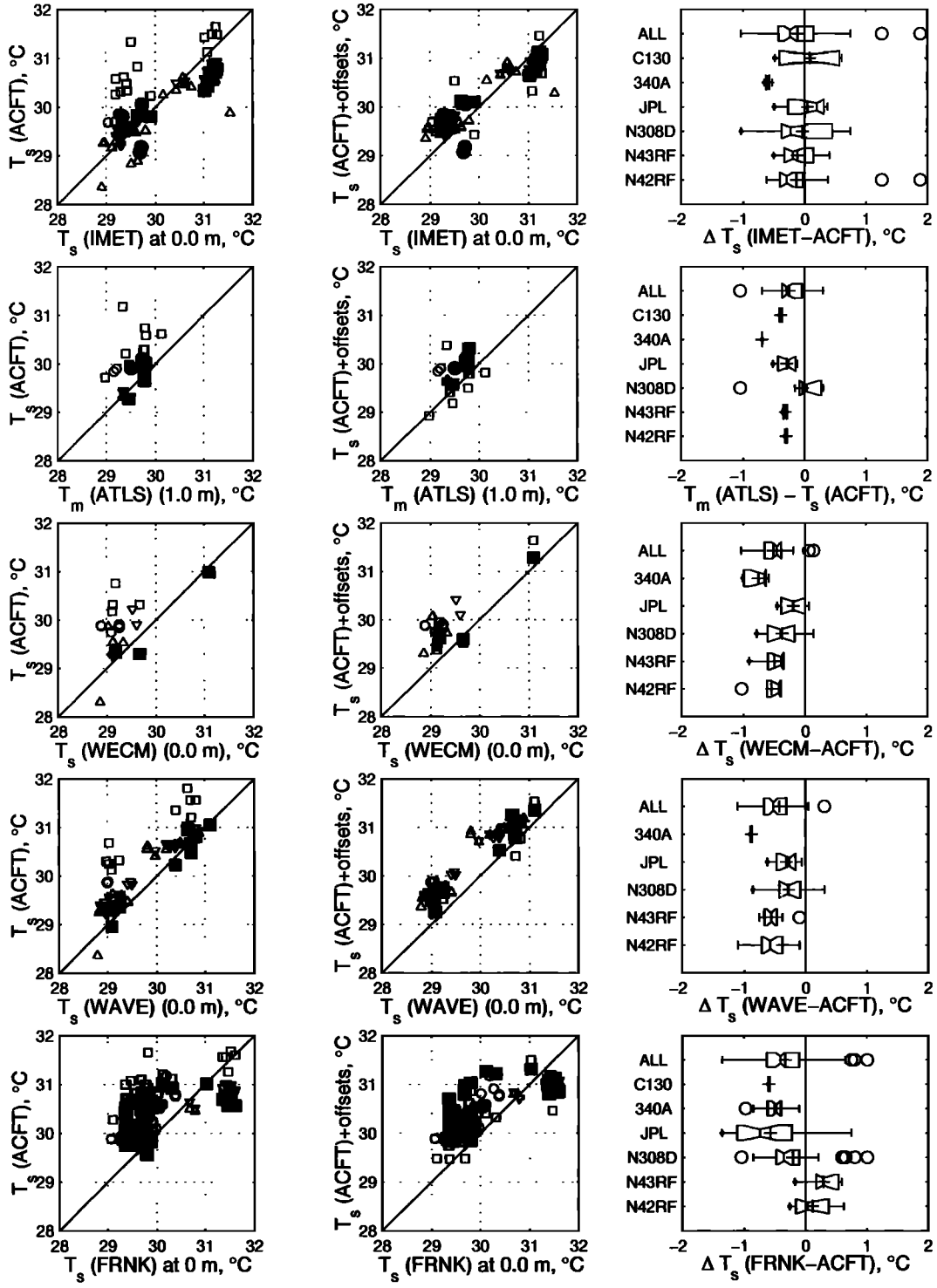

Figure 14. As in Figure 11 except that sea surface skin temperature T_s measurements are compared. Aircraft data are without (left), and with (middle) empirical corrections. *Franklin* T_s data are from the thermosalinograph.

due to the surface data being averaged over all daylight hours, whereas the aircraft data were from time periods when they were flying within the study area (about 3-4 hours). Even though this figure is not a strict comparison, it can be used to identify midday flights based on whether the aircraft Q_{SW} data were higher or lower than those from the surface platforms. The differences between the daytime-averaged *Moana Wave*, *Franklin*, *Wecoma* and IMET Q_{SW} and Q_{LW} measurements were reasonable.

For SST (Figures 17c1-17c2), the surface platform and aircraft data both resolve the large-scale trends during the IOP, and the agreement is reasonable. In Figures 17c1-17c2, the T_m and T_s data from IMET are

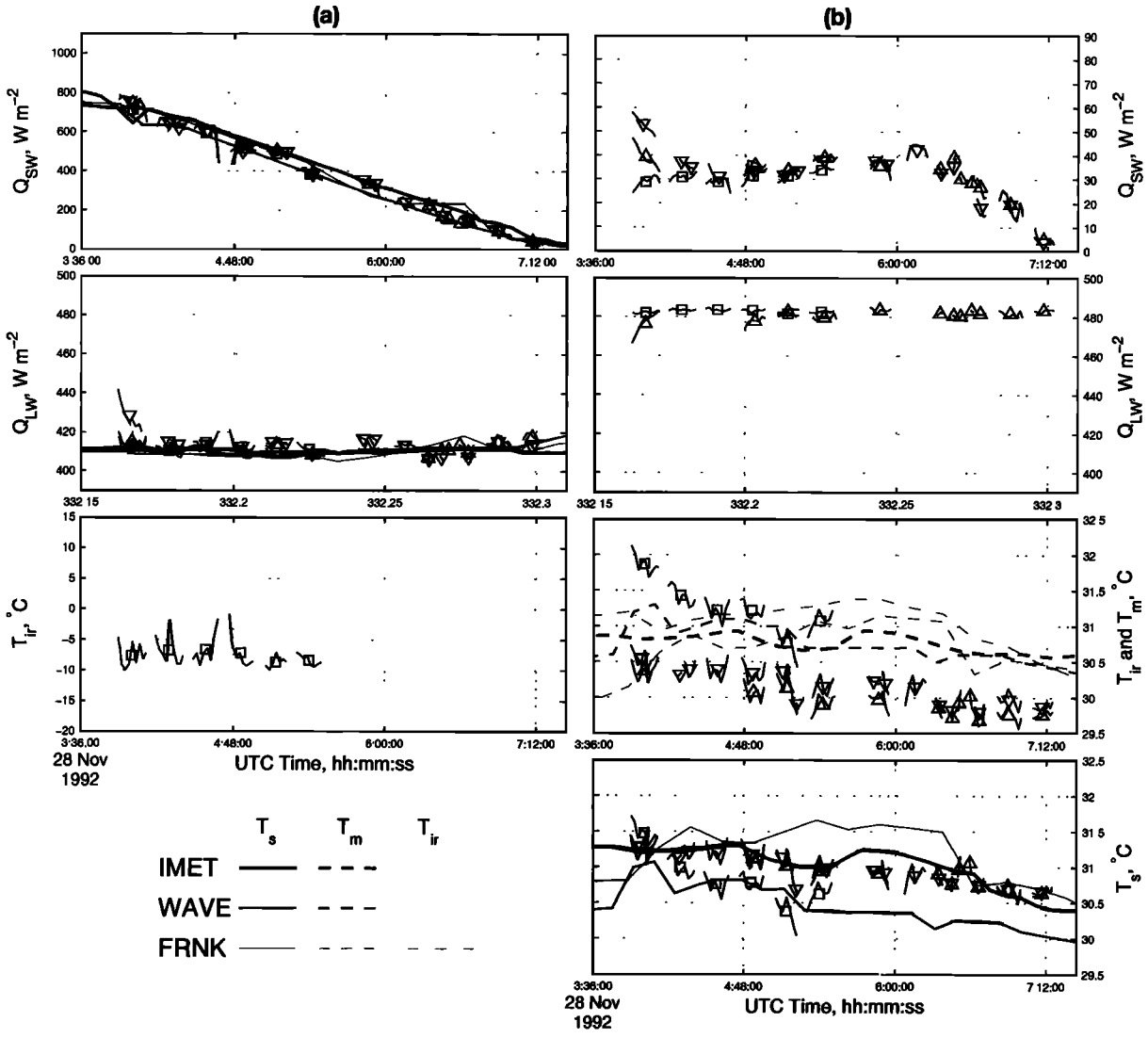

Figure 15. The 921128 time series of shortwave flux Q_{SW}, longwave flux Q_{LW}, indicated radiometric temperature T_{ir}, and sea surface temperature T_s measured by (a) upward looking and (b) downward looking sensors on surface platforms (continuous lines) and aircraft. The 10-km (short lines) and leg-long (symbols) mean values from aircraft data are shown. Aircraft are identified from Table 2 symbols. For surface platforms, see legend within the figure; for *Franklin* the T_{ir} data shown do not include the 0.4°C correction to account for emissivity and sky reflection.

both shown. The sharp spikes in the SST time series are diurnal warming events which occurred during time periods of low wind speed [see *Burns et al.*, 1999, Figure 19].

5.2. IOP Comparisons

For a more encompassing view of the comparison between the various platforms, all aircraft data were combined and compared with surface data from the same time periods. To do this comparison, all low-level data from the five aircraft (i.e., those shown in the frequency distributions of Figure 10) were combined to form the "aircraft" data set. On the basis of the times these aircraft were collecting low-level data, the ship and buoy data were conditionally selected to form the ship-combined and buoy-combined data sets. After interpolating the surface-platform data to a common sampling rate of 0.0167 Hz (1 sample/min) and only selecting every 30th aircraft data point, Figure 18 (row 4) shows the resulting frequency distributions. There were about 14,000, 13,200, and 16,900 samples for the aircraft-, ship-, and buoy-combined data sets, respectively. Surface platform data were also compared with each other (Figure 18, rows 2 and 3) and show similar measurement distributions. It should be noted that the aircraft radiative flux data set has slightly fewer values than that of the aircraft SST data set, due to previously described instrumentation problems with WP-3D PSPs and PIRs.

The agreement between the platforms appears to be reasonable, though the quantities (Q_{SW}, Q_{LW}, and T_s) measured by the aircraft have slightly higher values, es-

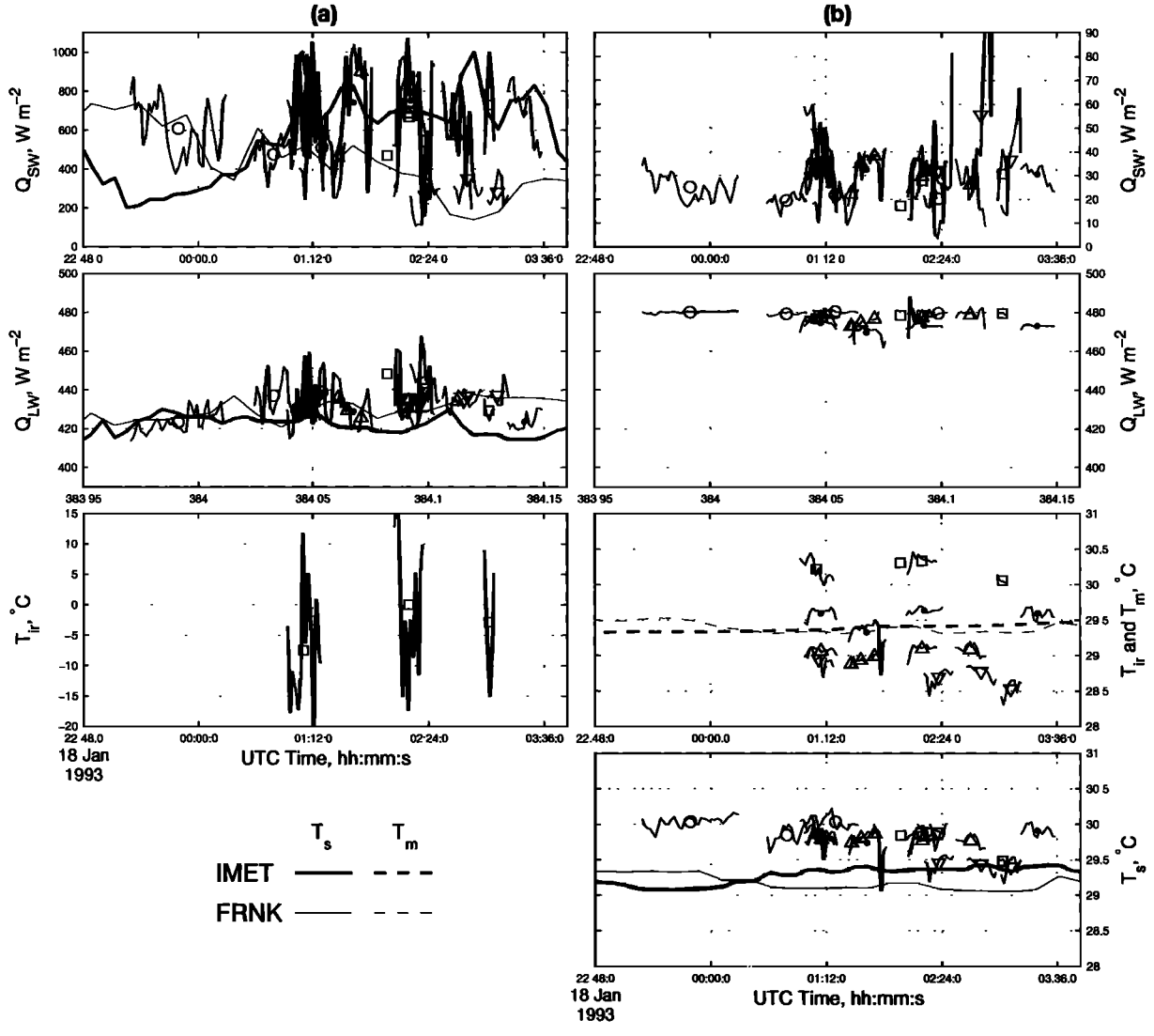

Figure 16. Same as Figure 15 but for the 930118 mission. Note the *Franklin* infrared radiometer was not working properly for this period.

pecially for T_s. It should be noted that missions with active convection did not generally include low-level runs; therefore most of the data in these frequency distributions are biased toward the calm, light-wind conditions often seen during COARE and are not a full representation of the range of conditions experienced throughout the IOP.

6. Discussion and Conclusions

Empirical corrections to the COARE aircraft radiation and SST measurements were determined from aircraft wingtip-to-wingtip, aircraft-ship, and aircraft-buoy comparison time periods. These corrections, which were flight-date-dependent for SST, reduce systematic measurement errors, produce a self-consistent aircraft data set, and improve the relative accuracy of the aircraft instrumentation (in many cases beyond the instrument specifications). This improvement is critical if aircraft data from multiple-aircraft missions are to be combined and used in detailed COARE analyses. Though aircraft wingtip-to-wingtip comparisons were useful in eliminating relative measurement differences between the aircraft, the absolute value of these corrections were determined with consideration of the comparisons between the aircraft and the surface-platform data. Measurement accuracy with and without the empirical corrections was estimated.

Prior to performing any comparisons, physically based corrections which account for aircraft attitude, elevation, and instrumentation time lags, were applied to the aircraft data. A new empirical approach for calibrating an Eppley pyrgeometer was introduced. On the basis of the large WP-3D PIR data set, this approach minimized the variance of Q_{LW}, as the empirical B coefficient in the equation for Q_{LW} was varied. By comparing the N42RF and C130 Q_{LW} data during level runs, it was concluded that the N42RF B values

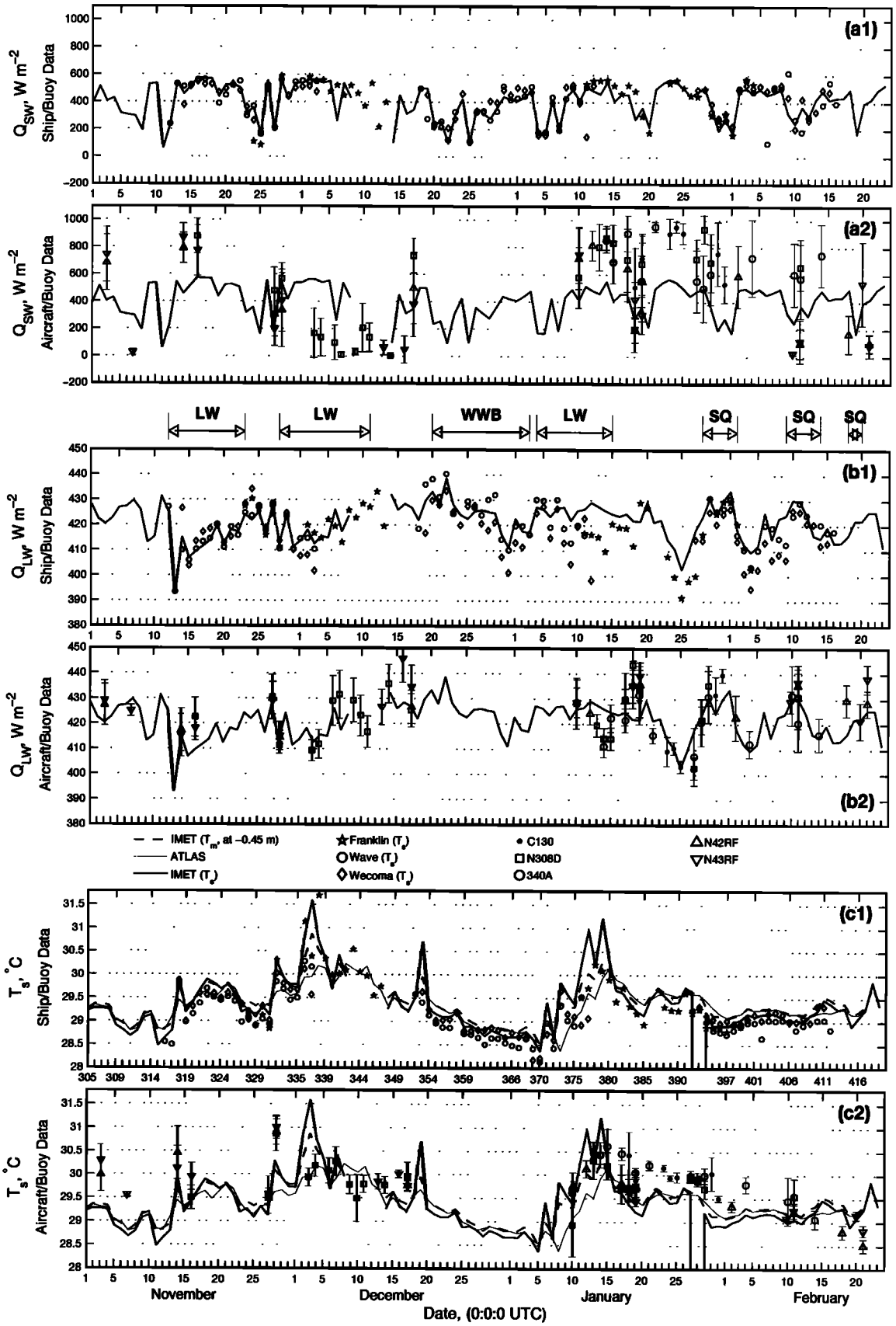

Figure 17. IOP time series of (a1-a2) downwelling shortwave flux Q_{SW}, (b1-b2) downwelling longwave flux Q_{LW}, and (c1-c2) sea surface skin temperature T_s. Figure legend is shown above c1. Buoy/ship data are in top panel, buoy/aircraft in bottom panel. Buoy and ship data are daylight-hour mean values, aircraft data are 10-km means with vertical bars representing the standard deviation of all 10-km mean values for the mission. Meteorological events, identified by vertical lines, are low-wind events (LW), westerly wind bursts (WWB), and squalls (SQ) as from *Weller and Anderson* [1996]. The Julian day, where 0 = 0000:00 UTC, January 1, 1992, is shown in Figure 17c1.

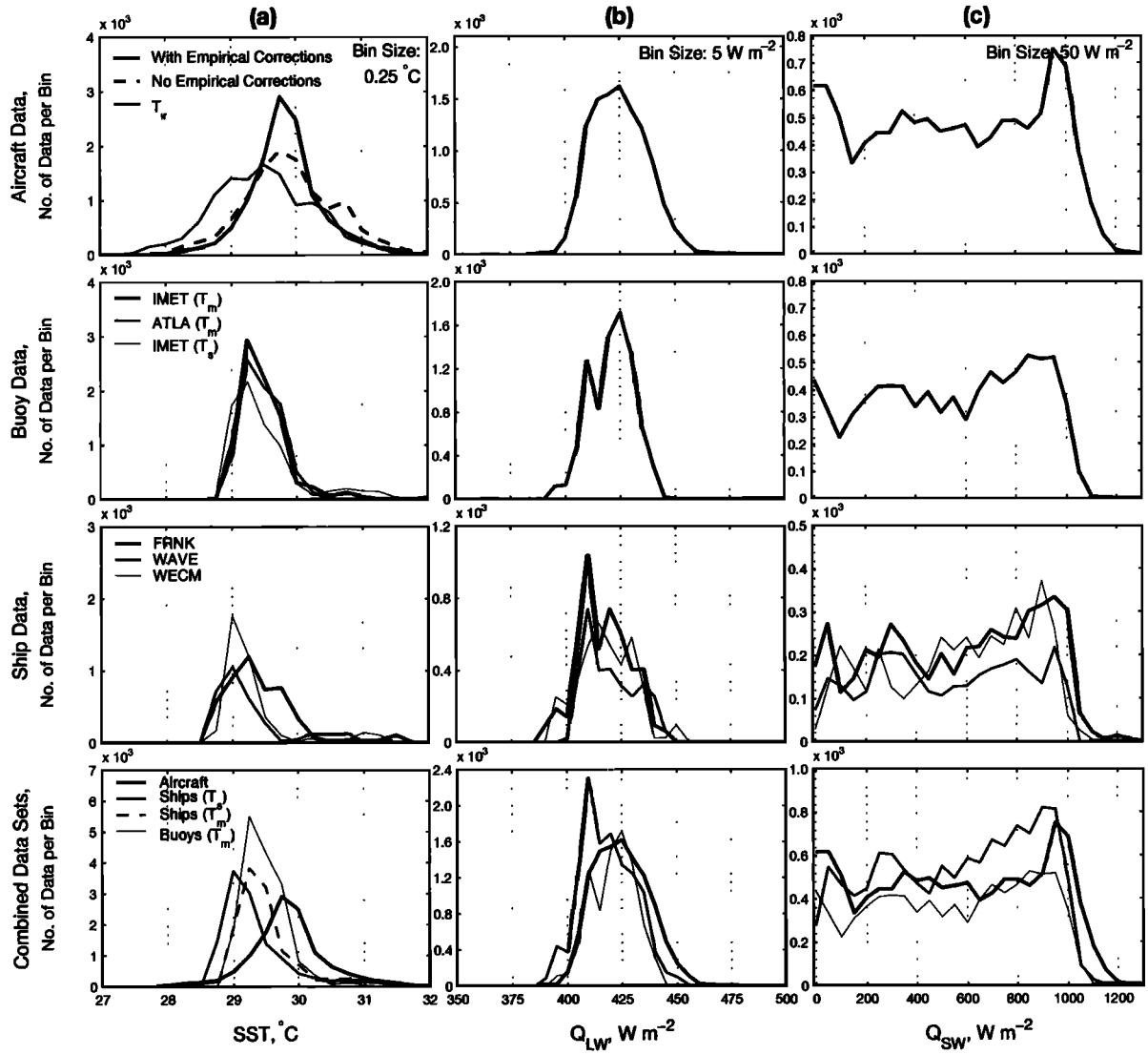

Figure 18. Frequency distributions of (a) sea surface temperature SST, (b) downwelling longwave flux Q_{LW}, and (c) downwelling shortwave flux Q_{SW} for all aircraft low-level run data. Unless otherwise specified, SST data are skin temperature (T_s) data. Buoy and ship frequency distribution data are from time periods between the start and the end of the aircraft low-level runs. See text for more information.

determined with this method removed small transients in the N42RF Q_{LW} data. Therefore the B values determined with the variance-minimization method were used in the WP-3D data processing.

Summary statistics (mean and standard deviation) from all five aircraft combinations (i.e., the aircraft that flew together during wingtip-to-wingtip comparison legs) are given in Table 5. To estimate the aircraft measurement accuracy, the mean of the absolute value of the mean difference for each aircraft combination is used. As an estimate of the random error in these measurements, the mean of the standard deviation of the difference for each of the five aircraft combinations is used (this value is shown after the plus-or-minus sign). It should be noted that aircraft involved in more comparison combinations (e.g., N42RF and N308D) have more influence on the resulting statistics. Before applying the empirical corrections to the aircraft data, the in situ accuracy of the downwelling shortwave and longwave irradiance is estimated to be 28±18 W m^{-2} and 9±4 W m^{-2}, respectively while that of SST is 0.7±0.4°C. After applying empirical corrections to these data, the relative accuracies improve to 3±16 W m^{-2}, 1±4 W m^{-2}, and 0.1±0.3°C, respectively. This table also compares the ensemble statistics of these data for the aircraft, ships, and buoys.

The use of empirical corrections to extend instruments beyond their specified accuracies is not the preferred method to account for inaccurate measurements. Ideally, the cause of systematic errors between instruments should be determined and in that way accuracy improved. Recent studies to improve the measurement of longwave radiation are a positive step in this direction [*Payne and Anderson*, 1999; *Fairall et al.*, 1998;

Table 5. Mean Radiation Measurement Accuracy Summary of Differences Among Aircraft Wingtip-to-Wingtip, Ships-Aircraft, and Buoys-Aircraft Comparison Data

		Measurement Differences					
		Figures 6 and 7	Figure 12		Ensemble Values, Figure 18; row 4		
Parameter (units)		Wingtip-to-Wingtip[a]	Ships-Aircraft	Buoys-Aircraft	Aircraft	Ships[b]	Buoys[c]
Q_{SW}, ($W\ m^{-2}$)	down-welling	3 ±16 [28 ±18]	-8 ±34	8 ±41	548 ±337	556 ±301	539 ±308
	up-welling	3 ±4 (no correction)			24 ±14		
Q_{LW}, ($W\ m^{-2}$)	down-welling	1 ±4 [9 ±4]	-3 ±5	-4 ±7	424 ±13	418 ±13	421 ±10
	up-welling	2 ±3 [5 ±3]			478 ±4		
SST, (°C)		0.1 ±0.3 [0.7 ±0.4]	-0.4 ±0.6	-0.1 ±0.4	29.8 ±0.6	29.5 ±0.5	29.5 ±0.3

Ensemble measurement statistics (mean ± standard deviation) are also given. See figure number(s) given in the second row for more information about data used to determine statistics. For parameters with two values, the upper values are with both physical and empirical corrections to aircraft data, and the lower values (enclosed in brackets) are using aircraft data with physical corrections, but no empirical corrections.

[a]Wingtip-to-wingtip aircraft accuracy is estimated by using statistics from all five wingtip-to-wingtip combinations. The first value is the mean of the absolute value of the mean differences between each pair (the absolute value is used so the result is independent of which aircraft is considered "reference" in taking the difference). The second value (shown after the "±") is the mean of the standard deviation of the mean difference for each combination.

[b]For the ships ensemble SST value, T_m data are used.

[c]Q_{SW} and Q_{LW} data are from IMET only; for the buoy SST ensemble value, IMET and ATLAS T_m data are used.

Philipona et al., 1998], and such studies should be encouraged.

Acknowledgments. We express gratitude to everyone who contributed to TOGA COARE data collection. We especially appreciate the long hours collecting data by flight crews and ship personnel aboard the NOAA WP-3Ds, NCAR N308D, FIAMS 340A, MRF C130, R/V *Franklin*, R/V *Moana Wave*, and R/V *Wecoma* as well as those involved in the IMET and Atlas buoy deployment. Special thanks to Bob Grossman (Aircraft PRTs), Ed Walsh (SSTs), Lynn deWitt (*Wecoma*), Meghan Cronin (Atlas), Mike McPhaden (Atlas), and Piotr Flatau (WP-3D PIRs) for their help. We also acknowledge the constructive comments from three anonymous reviewers. The work of S.P.B., D.K., and C.A.F. was supported by NSF grants ATM-9024436 and ATM-9110540 and NOAA grant 56GP0154-01. R.A.W. and S.P.A. were supported by NSF grant ATM-9525844. C.A.P. was supported by NSF grant OCE-9113510. This is contribution #10131 from the Woods Hole Oceanographic Institution.

References

Alados-Arboledas, L., J. Vida, and J. I. Jimenez, Effects of solar radiation on the performance of pyrgeometers with silicon domes, *J. Atmos. Oceanic Technol.*, *5*, 666-670, 1988.

Albrecht, B. A., and S. K. Cox, Procedures for improving pyrgeometer performance, *J. Appl. Meteor.*, *16*, 188-197, 1977.

Albrecht, B. A., M. Poellot, and S. K. Cox, Pyrgeometer measurements from aircraft, *Rev. Sci. Instrum.*, *45*, 33-38, 1974.

Bannehr, L., and V. Glover, Preprocessing of airborne pyranometer data, *NCAR Tech. Note TN-364+STR*, 35 pp., Natl. Cent. for Atmos. Res., Boulder, Colo., 1991.

Bannehr, L., and R. Schwiesow, A technique to account for the misalignment of pyranometers installed on aircraft, *J. Atmos. Oceanic Technol.*, *10*, 774-777, 1993.

Boers, R., R. M. Mitchell, and P. B. Krummel, Correction of aircraft pyranometer measurements for diffuse radiance and alignment errors, *J. Geophys. Res.*, *103*, 16,753-16,758, 1998.

Bradley, F., and R. Weller (Eds.), *Fourth Workshop of the TOGA COARE Air-Sea Interaction (Flux) Working Group, Woods Hole Oceanogr. Inst., Woods Hole, Mass., October 9-11, 1996*, Univ. Corp. for Atmos. Res., Boulder, Colo., 1997.

Burns, S. P., et al., Comparisons of aircraft, ship, and buoy meteorological measurements from TOGA COARE, *J. Geophys. Res.*, *104*, 30,853-30,884, 1999.

Coppin, P. A., E. F. Bradley, I. J. Barton, and J. S. Godfrey, Simultaneous observations of sea surface temperature in the western equatorial Pacific Ocean by bulk, radiative, and satellite methods, *J. Geophys. Res.*, *96*, 3401-3409, 1991.

Fairall, C. W., E. F. Bradley, J. S. Godfrey, G. A. Wick, J. B. Edson, and G. S. Young, The cool skin and warm layer in bulk flux calculations, *J. Geophys. Res.*, *101*, 1295-1308, 1996a.

Fairall, C. W., E. F. Bradley, D. P. Rogers, J. B. Edson, and G. S. Young, Bulk parameterization of air-sea flux-

es for Tropical Ocean Global Atmosphere Coupled-Ocean Atmosphere Response Experiment, *J. Geophys. Res., 101*, 3747-3764, 1996b.

Fairall, C. W., P. O. G. Persson, E. F. Bradley, R. E. Payne, and S. P. Anderson, A new look at calibration and use of Eppley Precision Infrared Radiometers. Part I: Theory and application, *J. Atmos. Oceanic Technol., 15*, 1229-1242, 1998.

Foot, J. S., A new pyrgeometer, *J. Atmos. Oceanic Technol., 3*, 363-370, 1986.

Glover, V., and L. Bannehr, Radiation measurements from NCAR aircraft, *NCAR Res. Aviat. Facil. Bull. 25*, 12 pp., Natl. Cent. for Atmos. Res., Boulder, Colo., 1993.

Godfrey, J. S., R. A. Houze, R. H. Johnson, R. Lukas, J.-L. Redelsperger, A. Sumi, and R.A. Weller, Coupled Ocean-Atmosphere Response Experiment (COARE): An interim report, *J. Geophys. Res., 103*, 14,395-14,450, 1998.

Grant, A. L. M., and P. Hignett, Aircraft observations of the surface energy balance in TOGA-COARE, *Q. J. R. Meteorol. Soc., 124*, 101-122, 1998.

Hagan, D., D. Rogers, C. Friehe, R. Weller, and E. Walsh, Aircraft observations of sea surface temperature variability in the tropical Pacific, *J. Geophys. Res., 102*, 15,733-15,747, 1997.

Hignett, P., Correction of airborne sea surface temperature measurements for non-blackness effects, *MRF Tech. Note 28*, 15 pp., Meteorol. Res. Flight, Hampshire, England, 1998.

Katsaros, K., Radiative sensing of sea surface temperature, in *Air-Sea Interaction: Instruments and Methods*, edited by F. Dobson, L. Hasse, and R. Davis, pp. 293-317, Plenum, New York, 1980.

Lambert, D., and P. Durand, Aircraft to aircraft intercomparison during SEMAPHORE, *J. Geophys. Res., 103*, 25,109-25,123, 1998.

LeMone, M. A., E. J. Zipser, S. B. Trier, The role of environmental shear and thermodynamic conditions in determining the structure and evolution of mesoscale convective systems during TOGA COARE, profile relationships in the atmospheric surface layer, *J. Atmos. Sci., 55*, 3493-3518, 1998.

Liu, W. T., and K. B. Katsaros, Spatial variation of sea surface temperature and flux-related parameters measured from aircraft in the JASIN experiment, *J. Geophys. Res., 89*, 10,641-10,644, 1984.

Payne, R. E., and S. P. Anderson, A new look at calibration and use of Eppley Precision Infrared Radiometers. Part II: Calibration and use of the Woods Hole Oceanographic Institution Improved Meteorology Precision Infrared Radiometer, *J. Atmos. Oceanic Technol., 16*, 739-751, 1999.

Philipona, R., C. Frohlich, and C. Betz, Characterization of pyrgeometers and the accuracy of atmospheric long-wave radiation measurements, *Appl. Opt., 34*, 1598-1605, 1995.

Philipona, R., et al., The Baseline Surface Radiation Network pyrgeometer round-robin calibration experiment, *J. Atmos. Oceanic Technol., 15*, 687-696, 1998.

Saunders, P. M., Aerial measurement of sea surface temperature in the infrared, *J. Geophys. Res., 72*, 4109-4117, 1967.

Saunders, P. M., Corrections for airborne radiation thermometry, *J. Geophys. Res., 75*, 7596-7601, 1970.

Saunders, R. W., and J. A. Barnes, Intercomparison flights of pyranometers and pyrgeometers on the MRF C-130, *MRF Int. Note 56*, 25 pp., Meteorol. Res. Flight, Hampshire, England, 1990.

Saunders, R. W., G. Brogniez, J. C. Buriez, R. Meerkötter, and P. Wendling, A comparison of measured and modeled broadband fluxes from aircraft data during the ICE '89 field experiment, *J. Atmos. Oceanic Technol., 9*, 391-406, 1992.

Serra, Y. L., Small-scale tropical cumulus cloud systems and the atmospheric boundary layer: An observational study, 180 pp., Ph.D. thesis, Univ. of Calif., San Diego, 1996.

Serra, Y. L., D. P. Rogers, D. E. Hagan, C. A. Friehe, R. L. Grossman, R. A. Weller, and S. P. Anderson, Atmospheric boundary layer over the central and western equatorial Pacific Ocean observed during COARE and CEPEX, *J. Geophys. Res., 102*, 23,217-23,237, 1997.

Song, X., and C. A. Friehe, Surface air-sea fluxes and upper ocean heat budget at 156°E, 4°S during the Tropical Ocean-Global Atmosphere Coupled Ocean-Atmosphere Response Experiment, *J. Geophys. Res., 102*, 23,109-23,129, 1997.

Valero, F. P. J., A. Bucholtz, B. C. Bush, S. K. Pope, W. D. Collins, P. Flatau, A. Strawa, and W. J. Y. Gore, Atmospheric Radiation Measurements Enhanced Shortwave Experiment (ARESE): Experimental and data details, *J. Geophys. Res., 102*, 29,929-29,937, 1997.

Vickers, D., and S. K. Esbensen, Subgrid surface fluxes in fair weather conditions during TOGA COARE: Observational estimates and parameterization, *Mon. Weather Rev., 126*, 620-633, 1998.

Walsh, E. J., et al., Observations of sea surface mean square slope under light wind during the Tropical Ocean-Global Atmosphere Coupled Ocean-Atmosphere Response Experiment, *J. Geophys. Res., 103*, 12,603-12,612, 1998.

Webster, P. J., and R. Lukas, TOGA COARE: The Coupled Ocean-Atmosphere Response Experiment, *Bull. Am. Meteorol. Soc., 73*, 1377-1416, 1992.

Weller, R. A., and S. P. Anderson, Surface meteorology and air-sea fluxes in the western equatorial Pacific warm pool during the TOGA Coupled Ocean-Atmosphere Response Experiment, *J. Clim., 9*, 1959-1990, 1996.

Williams, A. G., and J. M. Hacker, Description of instrumentation and flights conducted with FIAMS Cessna 340A aircraft "EOS" during the international experiment TOGA COARE, *Flinders Inst. Atmos. Mar. Sci. Tech. Rep. 10*, 65 pp., Flinders Univ. of South Australia, Adelaide, 1993.

Williams, A. G., H. Kraus, and J. M. Hacker, Transport processes in the tropical warm pool boundary layer. Part I: Spectral composition of fluxes, *J. Atmos. Sci., 53*, 1187-1202, 1996.

Williams, A. G., J. M. Hacker, and H. Kraus, Transport processes in the tropical warm pool boundary layer. Part II: Vertical structure and variability, *J. Atmos. Sci., 54*, 2060-2082, 1997.

S. P. Anderson and R. A. Weller, Physical Oceanography Department, MS 29, Woods Hole Oceanographic Institution, Woods Hole, MA 02543-1541. (sanderson@whoi.edu; rweller@whoi.edu)

E. F. Bradley and P. A. Coppin, CSIRO Land and Water, GPO Box 1666, Canberra, ACT 2601, Australia. (frank.bradley@cbr.clw.csiro.au; peter.coppin@cbr.clw.csiro.au)

S. P. Burns, C. A. Friehe, and D. Khelif, Department of Mechanical and Aerospace Engineering, University of California, Irvine, CA 92697-3975. (sean@ucar.edu; cfriehe@uci.edu; dkhelif@uci.edu)

C. W. Fairall, Environmental Technology Laboratory, NOAA, 325 Broadway, Boulder, CO 80303-3328. (cfairall@etl.noaa.gov)

A. L. M. Grant and A. G. Williams, Hadley Centre for Climate Prediction and Research, U.K. Meteorological Office, London Road, Bracknell, Berkshire RG12 2SY, United Kingdom.(almgrant@meto.gov.uk; awilliams@meto.gov.uk)

J. M. Hacker, Flinders Institute for Atmospheric and Marine Sciences, Flinders University, GPO Box 2100, Adelaide, SA 5001, Australia. (j.hacker@es.flinders.edu.au)

D. E. Hagan, Jet Propulsion Laboratory, MS 183-301, Pasadena, CA 91109. (Denise.E.Hagan@jpl.nasa.gov)

P. Hignett, Meteorological Support Group/DG(R&T), Ministry of Defence, Whitehall, London SW1A 2HB, United Kingdom. (phignett.msg.mod@gtnet.gov.uk)

C. A. Paulson, College of Oceanography, Oregon State University, Corvallis, OR 97331-5503. (paulson@oce.orst.edu)

D. P. Rogers, Marine Meteorology Research Group, Scripps Institution of Oceanography, La Jolla, CA 92093-0230. (drogers@ucsd.edu)

Y. L. Serra, Department of Atmospheric Science, University of Washington, Seattle, WA 98195-1640. (serra@pmel.noaa.gov)

(Received September 29, 1999; revised January 18, 2000; accepted February 3, 2000.)